Journal of Human Evolution 62 (2012) 377–394

Contents lists available at SciVerse ScienceDirect

Journal of Human Evolution

journal homepage: www.elsevier.com/locate/jhevol

Single-grain OSL chronologies for Middle Palaeolithic deposits at El Mnasra and El Harhoura 2, Morocco: Implications for Late Pleistocene human–environment interactions along the Atlantic coast of northwest Africa

Zenobia Jacobs [a,*], Richard G. Roberts [a], Roland Nespoulet [b], Mohammed Abdeljalil El Hajraoui [c], André Debénath [b]

[a] Centre for Archaeological Science, School of Earth and Environmental Sciences, University of Wollongong, Wollongong, NSW 2522, Australia
[b] Muséum national d'Histoire naturelle, Département de Préhistoire, UMR 7194, 75013 Paris, France
[c] Institut National de Sciences de l'Archéologie et du Patrimoine, 10001 Rabat, Morocco

ARTICLE INFO

Article history:
Received 25 May 2011
Accepted 5 December 2011
Available online 13 January 2012

Keywords:
Sand-sized quartz
Aterian
Sediment mixing
Dose distributions
MIS 5
Palaeoenvironments

ABSTRACT

Optically stimulated luminescence (OSL) measurements were made on individual, sand-sized grains of quartz from Middle Palaeolithic deposits at two cave sites (El Harhoura 2 and El Mnasra) on the Atlantic coast of Morocco. We were able to calculate OSL ages for 32 of the 33 samples collected from the Middle Palaeolithic deposits, including the earliest and latest Aterian levels at both sites. These ages reveal periods of occupation between about 110 and 95 ka (thousands of years ago), and at ~75 ka. A late Middle Palaeolithic occupation of El Harhoura 2 is also recorded at ~55 ka. Our single-grain OSL chronologies largely support previous age estimates from El Mnasra and other sites along the Atlantic coast of Morocco, but are generally more precise, reproducible and stratigraphically more coherent (i.e., fewer age reversals). We compare the single-grain ages for El Harhoura 2 and El Mnasra with those obtained from single- and multi-grain OSL dating of Middle Palaeolithic deposits in the nearby sites of Contrebandiers and Dar es-Soltan 1 and 2, and with records of past regional environments preserved in sediment cores collected from off the coast of northwest Africa. A conspicuous feature of the new chronologies is the close correspondence between the three identified episodes of human occupation and periods of wetter climate and expanded grassland habitat. Owing to the precision of the single-grain OSL ages, we are able to discern gaps in occupation during Marine Isotope Stages 5 and 4, which may represent drier periods with reduced vegetation cover. We propose that these climatic conditions can be correlated with events in the North Atlantic Ocean that exert a major control on abrupt, millennial-scale fluctuations between wet and dry periods in northwest and central North Africa.

Introduction

In recent years, there has been resurgence of research into the Middle Palaeolithic (MP) and Middle Stone Age (MSA) archaeological records of Africa. This is partly due to the widespread interest in issues relating to the origins of *Homo sapiens*, the dispersal of *H. sapiens* within, and out of, Africa, and the origins and development of modern human behaviour. The North African fossil evidence has been integrated into models dealing with origins of *H. sapiens* and their spread within Africa (Hublin et al., 1987; Hublin, 1992, 2001), with long-standing suggestions that the emergence of anatomical features particular to *H. sapiens* should not be restricted to sub-Saharan Africa (Hublin, 1992). By contrast, models dealing with the origins and development of modern human behaviour and the dispersal of *H. sapiens* out of Africa to populate the rest of the Old World are based largely on MSA finds and chronologies from sub-Saharan Africa (e.g., Jacobs and Roberts, 2008; Jacobs et al., 2008a).

The North African MP assemblages have rarely been integrated into such models, due to the low number of stratified Mousterian sites and the chronological uncertainties associated with the Mousterian and Aterian industries. From palaeoenvironmental records and geophysical data, it is now clear that the Sahara has not always been a biogeographic barrier between sub-Saharan and North Africa (e.g., Osborne et al., 2008; Drake et al., 2011), so it is important to construct a chronological framework for the MSA and MP assemblages in these regions to facilitate a pan-African synthesis of modern human evolution and migration. An improved understanding of the

* Corresponding author.
E-mail address: zenobia@uow.edu.au (Z. Jacobs).

0047-2484/$ – see front matter © 2011 Elsevier Ltd. All rights reserved.
doi:10.1016/j.jhevol.2011.12.001

timing, duration and (dis)continuity of these archaeological records, and their relation to changes in climate and environment, can help establish the sequence of events that may have led to certain key turning points in the history of *H. sapiens* populations both south and north of the Sahara.

Early *H. sapiens* in Morocco are associated with two MP industries, the Mousterian and Aterian. The Mousterian is similar to other Mousterian assemblages of the Near East and Europe: it is flake-based and displays some use of Levallois technology (McBurney, 1975; Bordes, 1976; Wendorf et al., 1993; Aumassip, 2001). It differs in other aspects of technology, however, and the assemblages are commonly deficient in retouched tools, with mainly side-scrapers. The Aterian industry includes elements not seen in Mousterian assemblages, such as stemmed artefacts (Reygasse, 1919–1920; Tixier, 1959), bifacial and unifacial points (Debénath, 1992; Marean and Assefa, 2005), worked bones (Ruhlmann, 1951; Howe, 1967; El Hajraoui, 1994), shell beads (Bouzouggar et al., 2007; d'Errico et al., 2009), pigment use (Nespoulet et al., 2008) and structured fireplaces (El Hajraoui, 2004; Nespoulet et al., 2008).

Recent dating projects in North Africa have specifically focussed on constraining the age of the Aterian, using four different techniques: optically stimulated luminescence (OSL) dating of sediments, thermoluminescence (TL) dating of burnt stones, electron spin resonance (ESR) dating of tooth enamel, and uranium-series dating of flowstone. Ages obtained using these methods indicate that the Aterian probably began well beyond the range of radiocarbon (^{14}C) dating, so the choice of an appropriate dating method is critical to resolving the antiquity of the Aterian (Wrinn and Rink, 2003; Bouzouggar et al., 2007; Mercier et al., 2007; Barton et al., 2009; Richter et al., 2010; Schwenninger et al., 2010).

Dating studies in Morocco have focussed on two geographic areas: 1) the Témara region on the Atlantic coast, which represents the westernmost extent of the known distribution of Aterian assemblages, and 2) the northeast region, inland from the Mediterranean coast (Fig. 1). The published ages for the Aterian (i.e., assemblages that contain stemmed pieces) appear to differ between these two regions, despite the same dating techniques being used. In the Témara region, the Aterian deposits at Dar es-Soltan 1 (Barton et al., 2009; Schwenninger et al., 2010), El Mnasra (Schwenninger et al., 2010) and Contrebandiers (Schwenninger et al., 2010; Jacobs et al., 2011) have OSL ages, all self-consistent, of between 123 ± 9 and 92 ± 6 ka (thousands of years ago). The oldest and youngest individual ages were obtained for samples OSL6 from Dar es-Soltan 1 (Level I) and SC31 from Contrebandiers (Layer 4d), respectively.

Much younger OSL ages (70 ± 4, 62 ± 4 and 59 ± 10 ka) have also been obtained for a second occurrence of the Aterian, higher up the stratigraphic profile at Dar es-Soltan 1 (in Ruhlmann's Layer C2; Barton et al., 2009) and at Contrebandiers (in Roche's Trench; Schwenninger et al., 2010), but see Jacobs et al. (2011) for a discussion of the reliability of the latter age estimate. These ages fall within the range of ages (85 ± 4 to 60 ± 5 ka) published for the Aterian at sites in northeast Morocco, including Taforalt (Bouzouggar et al., 2007), and for the proto-Aterian levels (Layer 3a) that underlie the undated Aterian levels (Layer 2) at Rhafas (Mercier et al., 2007). Bracketing ages of between 60 and 35 ka for the Aterian have also been reported for the site of Mugharet el 'Aliya, near Tangiers, based on ESR dating of tooth enamel (Wrinn and Rink, 2003). At Dar es-Soltan 1, the two discrete pulses of Aterian occupation (i.e., assemblages containing diagnostic stemmed points) were separated by layers with no stemmed points, and the same pattern was identified at Ifri n'Ammar. At the latter site, TL dating of burnt stones yielded weighted mean TL ages of 145 ± 9 and 83 ± 6 ka for the Aterian assemblages containing stemmed points (Richter et al., 2010).

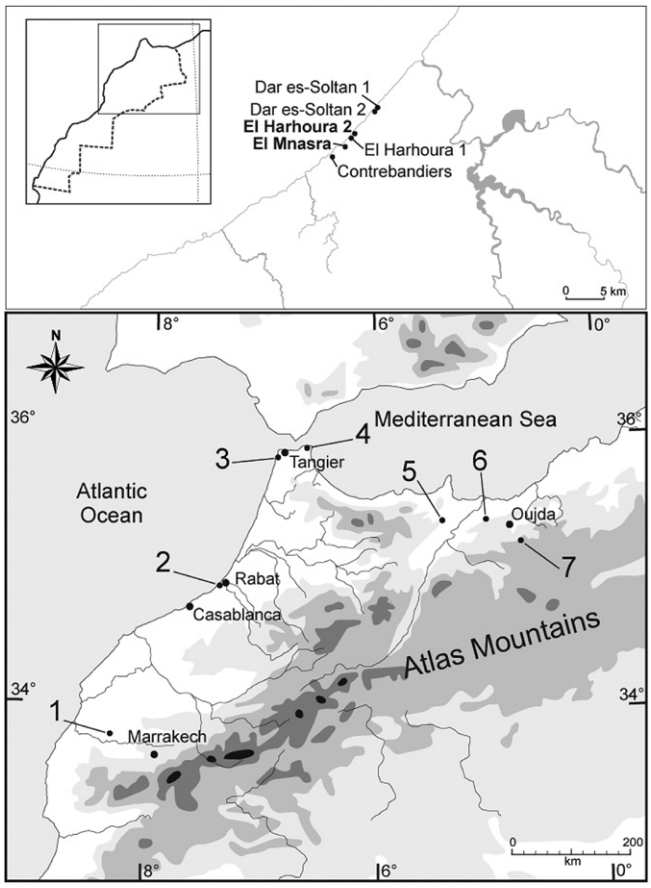

Figure 1. Map of northwest Africa indicating some of the better-known Middle Palaeolithic sites in Morocco: Djebel Irhoud (1), Témara (2), Mugharet el 'Aliya (3), Benzù (4), Ifri N'Ammar (5), Taforalt (6), Rhafas (7). The Témara region includes El Mnasra, El Harhoura 2 and several other sites referred to in this paper, which are marked on the detailed map in the top panel. The inset map shows the location of the geographic area enlarged in the bottom panel.

These new chronologies have implications for our understanding of the timing and culture-stratigraphy of the MP in North Africa. They re-introduce the question of which region of Africa, north of the Sahara, the Aterian originated in and dispersed from, and cast doubt on the Aterian as a single, short-lived culture. The revised chronologies challenge the consensus view, based on models of lithic assemblages and unreliable ^{14}C ages, that the Aterian on the Atlantic coast represents only the middle and later phases of this industry (Roche, 1969; Camps, 1974; Roche and Texier, 1976), and force a re-appraisal of the relationship between the Mousterian and Aterian, and the Aterian and Upper Palaeolithic (UP) Iberomaurusian. Furthermore, it is apparent from these recent studies, primarily of sites in Morocco (e.g., Bouzouggar et al., 2007; Nespoulet et al., 2008; Barton et al., 2009; Richter et al., 2010; Schwenninger et al., 2010), that the North African MP, and in particular the Aterian, can no longer be ignored in models of modern human behaviour and dispersal (Balter, 2011), but should be viewed as part of a pan-African MSA that represents one of the earliest fully modern behavioural adaptations (McBrearty and Brooks, 2000).

To address the implications raised by these recent studies requires an accurate and precise chronology for the entire MP throughout Morocco. Thus far, no single site appears to contain a continuous cultural sequence from the earliest to the latest MP, so finely-resolved dating comparisons between sites are needed. The necessary temporal resolution can only be achieved by conducting

a systematic dating study, using the same method, operator, equipment, measurement and analytical procedures for every sample. With this approach, systematic biases are held constant for all samples and the random component of error associated with subtle variations in sample preparation, measurement and data-analysis practices between different operators and laboratories can be minimized. Such a study may provide ages with the required reproducibility and precision to allow the identification of chronological patterns among sites, and enable comparisons with high-resolution palaeoclimatic data sets (e.g., Jacobs et al., 2008a), but it does not prevent replication of our study at one or many different sites by the same or other methods. Replication will address issues related to operator bias and measurement accuracy, but all sources of systematic error must be included in the uncertainties attached to the age estimates, which will reduce their precision and, thus, the ability to resolve subtle differences in timing.

In this paper, we use single-grain OSL dating as the method of choice and report its systematic application to the MP levels at two sites on the Atlantic coast (Témara region) of Morocco: El Mnasra and El Harhoura 2. Single-grain OSL dating has not been comprehensively used at any sites in North Africa, except for Contrebandiers (Jacobs et al., 2011). It was applied to three samples from Taforalt (Bouzouggar et al., 2007) and to some of the samples from Dar es-Soltan 1 (Barton et al., 2009), but without detailed supporting information. None of the reported ages for those two sites were based on these single-grain measurements. In the case of Contrebandiers, the first author of this paper (ZJ) also measured the majority of samples and analysed the data, so the ages from all three sites can be compared directly with the systematic component of error removed. By employing, in the same scientific program, the same method, equipment, procedures and operator in both studies, we can place El Mnasra, El Harhoura 2 and Contrebandiers on the common timescale developed originally for sites in southern Africa (Jacobs and Roberts, 2008; Jacobs et al., 2008a; Jacobs, 2010), and thereby improve the precision with which we can compare ages within and between regions, and calculate durations of particular industries.

The reason we have used single-grain OSL dating in this and previous studies is because of the benefits inherent in measuring individual grains from archaeological contexts where post-depositional disturbance may have occurred (Jacobs et al., 2006b, 2008c; David et al., 2007; Lombard et al., 2010) or where there is the possibility of roof spall contamination and other forms of inhomogeneous bleaching (Roberts et al., 1998, 1999; Jacobs et al., 2011). The incorporation of such 'contaminant' grains in a sample can skew the age estimate substantially, unless these grains are identified and removed prior to age calculation. This requires that grains are measured individually, rather than simultaneously as aliquots composed of many tens, hundreds or thousands of grains. The archaeological sediments at El Mnasra and El Harhoura 2 show potential for both of the major concerns discussed above: roof spall occurs in abundance in some units and localised disturbances have been documented in the form of pits dug by Neolithic and UP people into the underlying MP levels, and as large-scale animal burrows and smaller-scale insect activities (Nespoulet et al., 2008). The magnitude of impact that these factors may have on the reliable estimation of an OSL age will vary across a site, so each sample should be assessed individually. Multi-grain OSL dating can provide accurate results if grains with problematic behaviours are in the minority, or if there are no complications from post-depositional mixing or other forms of contamination. However, one cannot know beforehand if this is the case, hence the need for single-grain measurements. The purpose of this paper is to present the methodological and analytical information underpinning the single-grain OSL age estimates for these two sites, and thereby provide confidence in the chronologies derived for the MP levels.

Site background and stratigraphy

Since the 1940s, the archaeological discoveries made from sites near Rabat-Témara along the Atlantic coast have contributed to establishing Témara as a reference region for human occupation in North Africa. This is due to the large number of caves excavated within a restricted geographical area, extending ~9 km along the coastal strip between Rabat and Casablanca (Fig. 1). Sites include Dar es-Soltan 1 (Ruhlmann, 1951; Barton et al., 2009), Dar es-Soltan 2 (Debénath, 1975, 1976, 1980), El Harhoura 1 (Debénath and Shibi-Alaoui, 1979), El Harhoura 2 (Nespoulet et al., 2008), El Mnasra (El Hajraoui, 1993) and Contrebandiers (Roche, 1976; Roche and Texier, 1976). These caves occur within a low calcarenite cliff, which represents one of a series of dune cordons that runs parallel to the coast and is thought to have formed sometime during the Quaternary, when sea levels were higher than today. All of the caves face west, towards the ocean, which suggests that they were formed by sea erosion. However, the timing of dune deposition, subsequent carbonate cementation and cave formation are disputed. It had been thought that the dunes into which the caves are cut were of early Marine Isotope Stage (MIS) 5 age (130–110 ka; Texier et al., 1985), but preliminary OSL ages for samples of calcarenite indicate that the dunes may have formed at least ~210 ka, during MIS 7 (Barton et al., 2009), and possibly as early as MIS 11 (Jacobs et al., 2011).

The caves have acted as sediment traps, preserving thick accumulations of palaeontological (Monchot and Aouraghe, 2009), archaeological and culturally-sterile geological sediments. The cave deposits are 4.5–7.5 m deep and are dominated by sand derived mainly from disintegration of the host calcarenite, with some aeolian input (Niftah, 2003; Niftah et al., 2005; Nespoulet et al., 2008). The caves also present similar culture stratigraphies, with occupations during the Middle Palaeolithic, Upper Palaeolithic and Neolithic (early, middle and recent). Several of these caves also contain a wealth of *H. sapiens* remains associated with all major phases of occupation, including rare finds in the MP levels at Dar es-Soltan 2, El Harhoura 1 (Debénath, 1980, 2000), Contrebandiers (Roche, 1976; Balter, 2011) and, recently, at El Harhoura 2 and El Mnasra (El Hajraoui, 2004; ongoing study).

El Harhoura 2 El Harhoura 2 (33°95′N, 6°92′W) is located in the village of El Harhoura, ~4 km south of Rabat. It is situated ~300 m from the shore, and the top of the upper level is ~17 m above present sea level. The cave was first discovered in 1977 and after preliminary excavations in 1996, the site has been continuously excavated since 2001. The known extension of the cave is about 22 m wide, 9 m deep and 8 m high, and covers a total area of ~200 m^2 (Fig. 2a). Before excavations began, the cave was completely filled with sediments, and most were still preserved when excavation of a 2 m^2 test pit commenced in 1977, in the entrance of the cave. In 1996, a second 8 m^2 test pit established the depth of the three upper levels of deposits (Levels 1–3). The general archaeological sequence (Fig. 2a and b) was finally known in 2007 from a 4 m^2 test pit, although bedrock had still not been reached at a depth of 6.5 m. More laterally extensive excavations (25 m^2) have since been performed in the upper levels (1–4) in the entrance of the cave, and a 6 m^2 test pit has revealed an inner chamber at the back of the cave (Fig. 2a).

The stratigraphy currently comprises 11 levels (Fig. 2b), numbered from top to bottom. All levels are relevant to this paper, except for Level 1 (the Cardial, Middle and recent Neolithic) and Level 2 (the UP Iberomaurusian). Levels 5, 7, 9, 10 and 11 are archaeologically almost sterile, or have such low artefact densities that it is difficult to assign them to any particular culture. Levels 3, 4, 6 and 8 are classified as Aterian. No stemmed artefacts associated with the Aterian have been found in these assemblages, but all other attributes of the Aterian are represented. Levels 5–11 have

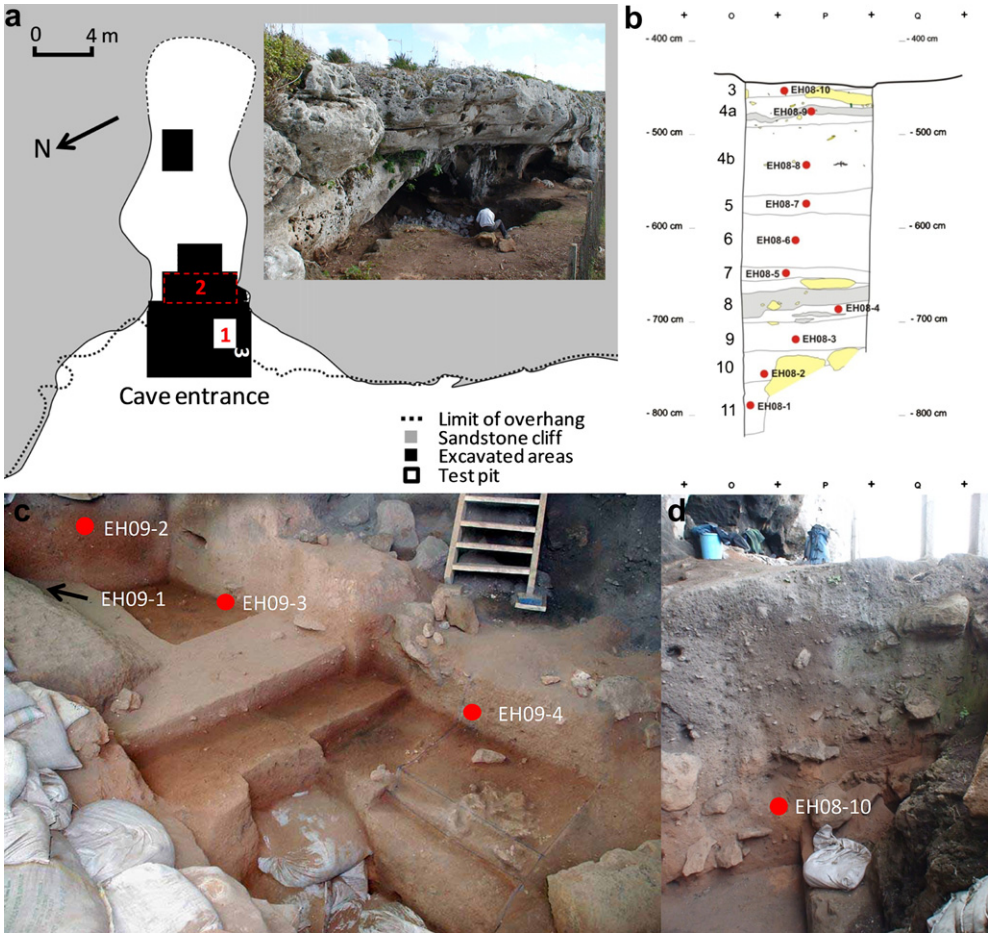

Figure 2. (a) Plan view of El Harhoura 2, showing the position of the test pit, the excavated areas and the position of the excavation in the rear cavity. The inset shows a general photograph of the cave in relation to the calcarenite cliff. The numbers 1–3 mark the general positions from where the OSL samples were collected from Levels 4a to 11. (b) Illustration of the test pit (Area 1 in Fig. 2a) and the position of each OSL sample and its identification code. (c) Photograph of Area 2 in Fig. 2a, showing the OSL sample positions and codes. (d) Photograph showing the position and code of the OSL sample collected from Area 3 in Fig. 2a.

been recognised only in the test pit (Fig. 2b), so the absence of stemmed points or pieces in Levels 6 (21 stone artefacts) and 8 (46 stone artefacts) may be due to the limited area of excavation. Further excavations are needed to obtain a larger archaeological sample before a definitive diagnosis can be made. The larger-scale, lateral excavations have revealed deposits representative of Levels 1–4 in front of the cave (Fig. 2c and d) and Levels 2 and 3 in the inner chamber. At the latter location, Level 3 is represented only by a ~10 cm-thick layer sitting on top of a rock, whereas Level 3 is well defined in front of the cave and yielded a comparatively large number of artefacts ($n = 286$). The absence of stemmed pieces in Level 3 and Level 4 (157 stone artefacts) may, therefore, imply an Aterian industry without these 'classical' pieces.

Preservation of micro- and macrofauna (Campmas, 2007; Stoetzel, 2009; Stoetzel et al., 2011a, b) is exceptional at El Harhoura 2, and includes human remains in Levels 1, 2, 3 and 8. Microvertebrate remains are abundant, compositionally diverse, and accumulated in situ as the result of predation by diurnal and nocturnal birds and small carnivores. The taphonomic study of Stoetzel et al. (2011b) demonstrated that these accumulations are almost undisturbed. The dominant macrofauna comprise the remains of various herbivores and carnivores (Michel et al., 2009, 2010), with the most hunted species being the gazelle (Campmas et al., 2008). Carnivores appear to have been the primary accumulator of mammal remains in Levels 3–5 (Campmas, personal communication).

To date, no ages have been published for the Middle Palaeolithic layers at El Harhoura 2.

El Mnasra El Mnasra (33°55′N, 6°57′W) is located in the town of Témara, and is positioned ~500 m from the shore and the surface of the deposits is ~14 m above current sea level. The cave is about 14 m wide, 22 m deep, 6 m high and covers a total area of 230 m^2 (Fig. 3a). The cave has a long history of archaeological research, starting with its discovery in the 1960s and continuing at the present day, involving the excavation of more than 100 m^3 of deposit. The stratigraphy currently comprises 12 levels, numbered from top to bottom (Fig. 3). Level 1 is a modern and disturbed sedimentary layer at the top of the sequence, while Levels 8, 9, 10 and 12 are archaeologically sterile. Level 2 is attributed to the Cardial Neolithic, Level 3 is assigned tentatively to the Iberomaurusian, and Levels 4–7 and 11 are classified as Aterian. In contrast to El Harhoura 2, stemmed pieces were recovered from all Aterian levels. The latter also contain evidence of closed fireplaces (with edges defined clearly by limestone pavements) and open hearths of oval and circular shape (El Hajraoui, 2004). Bone tools (El Hajraoui, 1993, 2004) and worked hematite (Nespoulet et al., 2008) have been recovered from the Aterian levels, along with concentrations of *Nassarius* shell beads (many of which are perforated), similar to those reported for Taforalt (Bouzouggar et al., 2007) and other sites in North Africa, the Near East and South Africa (Henshilwood et al., 2004; Vanhaeren et al., 2006; d'Errico et al., 2009). The micro- and macrofaunal records

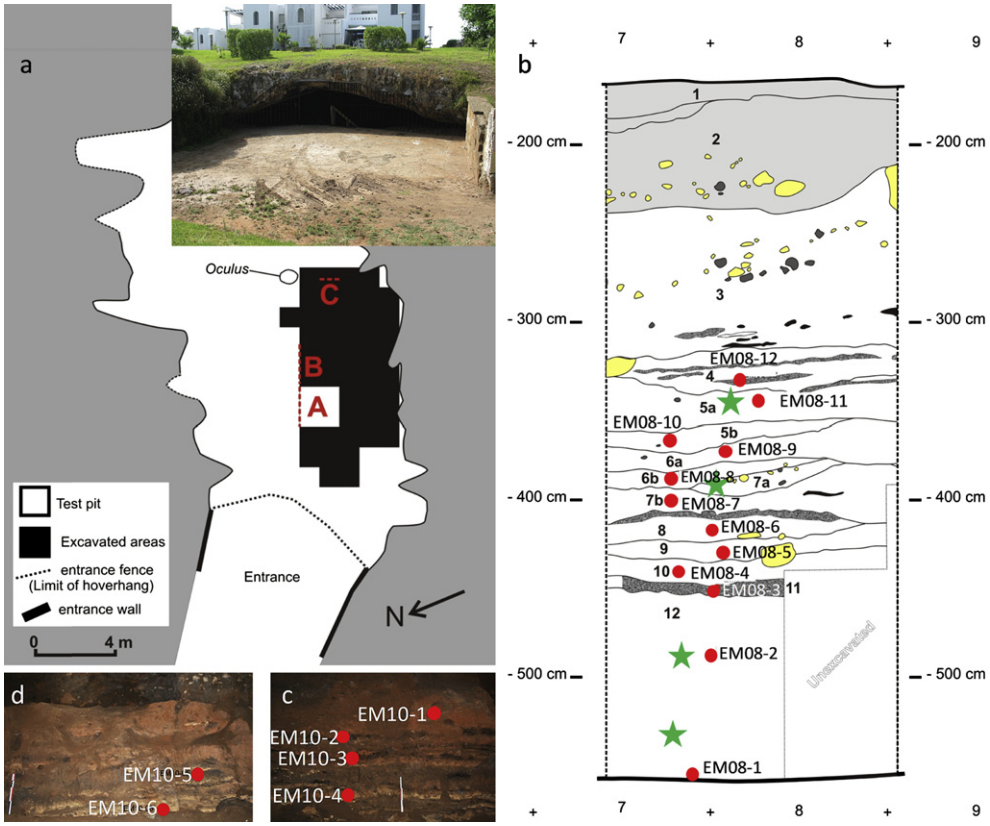

Figure 3. (a) Plan view of El Mnasra, showing the position of the test pit (Area A) and the excavated areas (black squares). The inset shows a photograph of the cave entrance in relation to the calcarenite cliff. The letters A–C show the general position from where the various OSL samples were collected. (b) Illustration of the test pit (Area A in Fig. 3a.) and the position of each OSL sample and its identification code. The samples are numbered in reverse stratigraphic order from EM08-1 at the base (Level 12) to EH08-12 near the top (Level 4). The stars indicate the positions of the four samples reported in Schwenninger et al. (2010). (c) Photograph of Area B in Fig. 3a, showing the positions and codes of OSL samples collected from Level 3. (d) Photograph of Area C in Fig. 3a, showing the position and codes of additional OSL samples collected from Level 4.

at El Mnasra are similar to those at El Harhoura 2, and isolated human remains have been found with the Aterian in Levels 5 and 6.

To date, four multi-grain OSL ages have been obtained for the sedimentary deposits at El Mnasra (Schwenninger et al., 2010). These suggest deposition of the lowermost sediments (Level 11) during or shortly after MIS 5e (119 ± 20 and 112 ± 7 ka), and occupation of the site during the Aterian at 108 ± 8 ka (Level 7b) and 106 ± 12 ka (Level 5a).

In summary, the MP sequences of the two sites are very similar. Both are characterised by low artefact densities and similar raw material sources (mainly quartzite, flint and exogenous limestone), and the micro-Levallois débitage (flakes and cores), types of side scrapers and other retouched tools are identical in the two caves. The only major difference is the marked absence of stemmed pieces from the Aterian assemblages at El Harhoura 2. The absence of stemmed pieces, however, is not sufficient to infer a cultural distinction between the two Aterian sequences until their contemporaneity has been established and further collections made at El Harhoura 2. This caveat also extends to the MP deposits at Contrebandiers and Dar es-Soltan 1 and 2. In this paper, therefore, all MP deposits from sites in the Témara region are referred to as Aterian. We are not concerned here with the re-appraisal of the cultural definition of the artefact assemblages—the cultural attributions of individual levels, and correlations between assemblages from different sites, are the subject of papers in preparation and of new studies that are underway. This paper addresses the chronological question, our aim being to provide a standardised timeframe that will enable archaeologists to make direct comparisons between contemporaneous assemblages from different sites.

Sampling for OSL dating

A total of 30 samples, 15 each from El Harhoura 2 and El Mnasra, were collected from the MP levels for OSL dating. Both archaeological and non-archaeological levels were sampled, the latter to provide additional chronological and contextual information. A further nine samples were collected from deposits attributed to the UP. Dating of the UP deposits at El Harhoura 2 will be discussed elsewhere, but the three samples collected from the purported UP at El Mnasra are reported here, because we provide evidence that the host sediments are not, in fact, associated with the UP.

Each sample was collected by hammering opaque plastic tubes (5 cm in diameter and 15 cm in length) into the cleaned section walls. Extra material was collected for laboratory-based radioactivity measurements and to determine the field moisture content of each sample. At least one OSL sample was collected from each stratigraphic layer, with the majority of samples collected from a single stratigraphic profile at each site (Figs. 2b and 3b).

Owing to the nature of the Level 3 deposits at El Harhoura 2, however, it was necessary to collect multiple samples from across a wide area. This level was heavily altered by pit-digging and bioturbation in places, especially along the eastern wall of the cave, so by sampling strategically we hoped to obtain more accurate age estimates from the areas that had been altered least. At El Mnasra, Level 4 thickened considerably to the back of the cave, where it consisted of multiple white ash bands. To capture this change, sediments from the uppermost and lowermost exposed ash bands were sampled along the North face. The sample positions, their stratigraphic levels, and archaeological associations are shown in Figs. 2 and 3.

Age determination by OSL dating

OSL dating provides a means of determining burial ages for sediments. The time elapsed since sediments were last exposed to sufficient heat or sunlight to reset the luminescence 'clock' can be estimated from measurements of the OSL signal, and of the radioactivity of the sample and surrounding materials (Aitken, 1998; Bøtter-Jensen et al., 2003). By measuring the OSL signal from a sample of sediment, the equivalent dose (D_e) can be determined. The D_e is defined as the amount of radiation (in gray, Gy) needed to generate an OSL signal in the laboratory of equal intensity to that emitted by the natural sample as a result of the sediment grains having been exposed to low levels of ionizing radiation in the natural environment after the most recent 'clock' resetting event. In practice, this involves comparing the OSL signal from the natural sample with the signals induced in the laboratory by administering known doses (using a calibrated radiation source) to portions of the same sample (in this study, individual grains). The latter signals are used to construct an OSL dose–response curve (Fig. 4), from which an estimate of the D_e can be made.

An estimate of the environmental dose rate (D_r) is also required to determine an OSL age. The D_r represents the rate of supply of ionizing radiation to the sample in the natural environment over the entire period of burial. This involves assessing the radioactivity of the sample and the surrounding material, to a distance of about 40 cm, using chemical or physical methods. An estimate of the time of burial of fully bleached or heated grains can then be obtained by dividing the D_e by the D_r.

Recent reviews of the method as applied to archaeological materials can be found in Feathers (2003a), Jacobs and Roberts (2007), and Wintle (2008).

Sample preparation and OSL instrumentation

All samples were opened in the laboratory under appropriate lighting conditions (dim red/orange illumination). Sediments collected for moisture content and radioactivity measurements were weighed and dried to obtain estimates of field moisture content, and these same sediments were then ground to a fine powder for laboratory determinations of the D_r. All OSL samples were subjected to a series of chemical treatments to isolate quartz grains of a specific size range for measurement of the OSL signal. Carbonates were dissolved in 10% HCl acid, and organic matter was oxidized in 30 vol H_2O_2. The 180–212 μm diameter grain-size fraction was then separated by wet sieving and the quartz grains isolated by density separation, using sodium polytungstate solutions of specific gravity 2.62 (to reduce the potassium-rich feldspar content) and 2.70 (to remove heavy minerals). The quartz grains were etched in 40% HF acid for 45 min to destroy any remaining feldspars, and then washed with concentrated HCl acid for 45 min to remove any precipitated fluorides. The etched quartz grains were sieved again, using the smaller mesh diameter (180 μm), and only grains retained on this sieve were used for dating. This same procedure was systematically applied to each sample, and generated ample material in all cases.

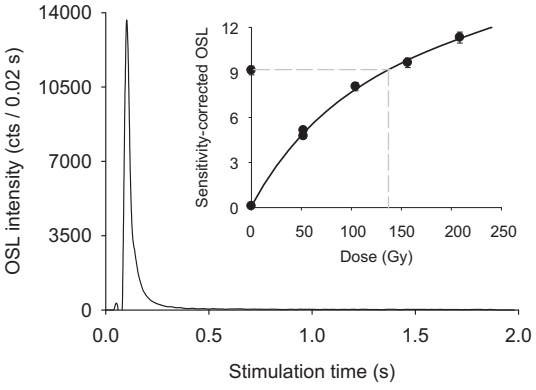

Figure 4. OSL decay and dose–response curves for a representative single grain from El Mnasra. This grain is typical of those accepted for D_e determination after application of stringent data rejection criteria to eliminate grains with unsuitable OSL characteristics.

The prepared quartz grains were mounted on discs that had a 10 × 10 grid of 300 μm diameter holes drilled in the surface, so that each hole contained one grain of ~200 μm in diameter. In total, 31,400 grains were measured individually in this way. A Risø TL/OSL-DA-15 optical stimulation and detection system, equipped with a focussed laser attachment for optical stimulation of individual sand-sized grains, was used to measure each grain in this study. OSL measurements were made using the beam from a 10 mW Nd:YVO_4 diode-pumped green laser (532 nm) focussed to a 10 μm diameter spot with a power density of ~50 W/cm^2 (Bøtter-Jensen et al., 2000). The laser reproducibility on our instrument was estimated to be ±2%, which we have propagated through the error calculation for each of the natural, regenerative and test dose OSL signals. The ultraviolet OSL emissions were detected using an Electron Tubes Ltd 9635Q photomultiplier tube fitted with 6 mm of Hoya U-340 filter, and laboratory doses were given using a $^{90}Sr/^{90}Y$ beta source mounted on the reader. The beta source was calibrated using a range of known gamma-irradiated quartz standards and to account for spatial variation in dose across a disc (e.g., Ballarini et al., 2006), we determined the beta dose rates to individual grain positions from measurements of gamma-irradiated quartz grains.

Equivalent dose measurements

The measurement procedures employed in this study are the same general single aliquot regenerative-dose (SAR) procedures as those described in Jacobs et al. (2003b, 2006b, 2008a, c) for single grains. After measurement of the natural OSL signal, each grain was subjected to seven regenerative-dose cycles, and the induced OSL signals were measured. These cycles included laboratory doses of between 30 and 320 Gy, a duplicate dose and a zero dose, which form part of the SAR performance tests routinely carried out on quartz grains (Jacobs and Roberts, 2007). After measurement of the natural and each regenerative dose, a fixed test dose of ~9 Gy was applied and then optically stimulated. The resulting OSL signal was used to monitor and correct for any sensitivity changes between successive SAR cycles. The natural and regenerative doses were preheated at 180 °C for 10 s, and the test doses at 180 °C for 5 s, before optical stimulation for 2 s at 125 °C (at 90% laser power). The OSL signal was determined from the first 0.22 s of stimulation, and the count rate over the final 0.33 s was used as background. At the end of this SAR sequence, a check was also made for the presence of infrared-sensitive grains and inclusions, using the OSL IR depletion-ratio test described by Jacobs et al. (2003a) and Duller (2003). A representative OSL decay curve and dose–response curve for a single grain of quartz from El Mnasra are shown in Fig. 4.

As reported in previous studies, not every grain yields useful information on absorbed dose (Jacobs and Roberts, 2007). Accordingly, we rejected uninformative grains (Tables S1–S4) using objective criteria described and tested elsewhere (Jacobs et al., 2003a, 2006a). These included the rejection of grains with (1) an initial OSL signal from the first test dose of less than three times the background count rate; (2) a sensitivity-corrected signal measured in the zero-dose cycle of more than 5% of the sensitivity-corrected natural OSL signal; (3) a 'recycling ratio' between the sensitivity-corrected

signals for the duplicate regenerative doses that differed significantly (i.e., at 2σ) from unity; (4) a sensitivity-corrected natural OSL signal that did not intercept the dose–response curve ('over-saturation'); and (5) an OSL IR depletion-ratio smaller than unity by more than 2σ.

Most grains were rejected owing to the lack of a discernible OSL response to the test dose (criterion 1), which provides information about the inherent brightness of a grain. It is common in studies of quartz grains from a range of geographic and depositional environments that a large proportion of measured grains are not luminescent. Based on our experience, the grains from El Mnasra and El Harhoura 2 are some of the more luminescent observed. For the majority of samples, more than 50% of the grains produced a measurable OSL signal. This high OSL sensitivity to dose was also noted for the samples from Dar es-Soltan 1 (Barton et al., 2009).

It is also noteworthy that a large number of grains were rejected for some samples because the sensitivity-corrected natural signal (L_N/T_N) did not intercept the dose–response curve (criterion 4). These grains are 'over-saturated' and are an experimental artefact that is not well understood (Yoshida et al., 2000; Bailey, 2004; Bailey et al., 2005; Jacobs et al., 2006b). Multi-grain aliquots will include an unknown proportion of such grains, which will contribute to the measured OSL signal and may result in a significant overestimation of D_e and, hence, age.

For grains that satisfied the criteria for acceptance, a saturating-exponential-plus-linear curve was fitted to the regenerative-dose points and the D_e was obtained from interpolation of the natural signal (Fig. 4). Under the measurement conditions specified above, this procedure gave correct estimates of dose for single grains of samples EH08-3 and EM08-5 that had been bleached in sunlight and then given a known dose of 100 Gy, similar to that expected for the burial doses of the majority of our samples. Both samples had mean ratios of measured/given dose consistent with unity—1.03 $\pm$ 0.06 (n = 163) and 0.98 $\pm$ 0.05 (n = 127), respectively—but the individual dose estimates were spread more widely than expected from their measurement uncertainties alone, yielding 'overdispersion' values (Roberts et al., 2000) of 12 $\pm$ 2 and 15 $\pm$ 2%, respectively. This extra spread is typical for sedimentary quartz grains, even in the absence of any complicating factors such as insufficient sunlight exposure before burial or sediment mixing after burial, and should be taken into account when D_e distributions for natural samples are assessed for the effects of depositional and post-depositional processes.

Dose recovery tests were also performed using alternative preheat treatments, which revealed that the samples from these two sites are largely insensitive to the typical range of preheat temperatures used in OSL dating. The measurement conditions employed in this study are also consistent with those independently assessed for quartz grains extracted from deposits in nearby Contrebandiers (Jacobs et al., 2011).

In addition to the presence of 'over-saturated' grains in the El Mnasra and El Harhoura 2 deposits, we identified a variety of other quartz OSL characteristics that are not favourable for D_e determination. For example, many of the grains exhibited unusually slow rates of OSL decay with stimulation time, which suggests the presence of a large, hard-to-bleach component in the OSL signal. The vast majority of grains with this and other aberrant luminescence characteristics failed to satisfy one or more of the aforementioned objective criteria and were therefore rejected during the initial screening process. We also scrutinised each of the remaining grains individually before calculating the D_e, but did not find any reasons to reject additional grains. The majority of accepted grains were characterised by OSL signals that decayed rapidly with stimulation time, consistent with them being composed predominantly of the most light-sensitive ('fast') component of quartz OSL, and produced dose–response curves typical for quartz (Fig. 4). In addition, none of the grains showed significant variation in D_e when the signal integration range was systematically changed to construct $D_e(t)$ plots (e.g., Bailey, 2003). This suggests that even the few grains with slower rates of OSL decay had been fully bleached prior to burial, and are not afflicted by the differential rates of sensitivity change reported for the various OSL components present in other quartz samples (e.g., Jain et al., 2003; Singarayer and Bailey, 2003). Because of the favourable luminescence characteristics of these grains, we consider that the D_e values and OSL ages obtained from them will provide useful and reliable information about the depositional and post-depositional history of the sediments.

Analysis and interpretation of D_e distributions

Of the 31,400 individual sand-sized grains of quartz measured, between 11% and 43% of grains per sample proved suitable for OSL dating using the SAR procedure (Tables S1–S4). In total, D_e values were estimated for 9424 grains (30% of the number of grains measured), and these are displayed as radial plots in Figs. S1 and S2 for each of the samples from El Harhoura 2 and El Mnasra, respectively. In such plots, the most precise estimates fall to the right and the least precise to the left. If the D_e values are consistent with statistical expectations, then 95% of the points should scatter within any chosen band of width $\pm$2 units projecting from the left-hand (standardised estimate) axis (Galbraith et al., 1999).

The grey shaded bands in Figs. S1 and S2 are each $\pm$2 units in width, so it is immediately apparent that for all samples, the D_e estimates are spread too widely to fall within any single shaded band. This is reflected also in the overdispersion values of 21–43% (El Harhoura 2: Table 1) and 18–89% (El Mnasra: Table 2), which are much greater than the values obtained for samples EH08-3 and EM08-5 under controlled laboratory conditions in the dose recovery test. We attribute this additional D_e overdispersion to the samples being afflicted by variations in the beta dose rate to individual grains (e.g., Murray and Roberts, 1997; Olley et al., 1997) and/or by post-depositional mixing of grains with different burial ages (e.g., Roberts et al., 1998, 1999; Feathers, 2003b; Jacobs et al., 2006b, 2008b; David et al., 2007; Lombard et al., 2010; Tribolo et al., 2010). We refer to the two types of D_e distributions resulting from the influence of these factors as 'scattered' and 'mixed', respectively, following the nomenclature introduced by Jacobs et al. (2008b) for samples from Sibudu, South Africa. We reserve the term 'mixed and scattered' for distributions affected by both beta dose variations and post-depositional mixing; these D_e distributions were treated as 'scattered' after removing the intrusive grains.

The finite mixture model (FMM) was applied to both types of single-grain D_e distribution to determine the number of discrete D_e components, the relative proportion of grains in each component, and the weighted mean D_e value and associated standard error of each component (Roberts et al., 2000; David et al., 2007; Jacobs et al., 2008c, 2011). We ran the FMM using overdispersion values of between 10 and 20% and identified the minimum number of statistically supported D_e components from the values of maximum log likelihood and the Bayes Information Criterion (BIC). Details about the number of components, their relative proportions, and their weighted mean D_e values are listed for each of the samples in Table 1 (El Harhoura 2) and 2 (El Mnasra). Jacobs et al. (2011) give worked examples for samples from the nearby site of Contrebandiers, and Jacobs and Roberts (2007) provide further discussion on the interpretation of radial plots and a review of the FMM and other age models.

The standard error in D_e obtained using the FMM represents the total uncertainty associated with all sources of random variation arising from photon counting statistics, instrument reproducibility

Table 1
D_e information for all samples measured from El Harhoura 2.

Sample	Excavation level	No. of grains	Central D_e (Gy)	Overdispersion (%)	No. of components[a]	D_e values (Gy) and proportions (%)					
						Component-1		Component-2		Component-3	
						D_e	Proportion	D_e	Proportion	D_e	Proportion
EH08-1	11	296	111 ± 2.3	24 ± 2	2 (s)	46.4 ± 7.5	2.6 ± 1.5	**114.0 ± 2.3**	**97.4 ± 1.5**		–
EH08-2	10	303	112 ± 2.2	23 ± 2	2 (s)	67.1 ± 6.3	7.3 ± 3.5	**117.0 ± 2.7**	**92.7 ± 3.5**		–
EH08-3	9	294	111 ± 2.1	21 ± 2	2 (s)	52.3 ± 10.7	1.6 ± 1.5	**112.7 ± 2.1**	**98.4 ± 1.5**		–
EH08-4	8	239	98 ± 2.2	25 ± 2	2 (s)	66.5 ± 7.2	14.8 ± 8.2	**105.8 ± 3.5**	**85.2 ± 8.2**		–
EH08-5	7	333	91 ± 1.7	25 ± 2	2 (s)	59.7 ± 6.7	12.2 ± 6.5	**93.7 ± 2.6**	**87.8 ± 6.5**		–
EH08-6	6	264	86 ± 1.8	26 ± 2	2 (s)	51.3 ± 4.1	12.1 ± 4.1	**91.8 ± 2.2**	**87.9 ± 4.1**		–
EH08-7	5	219	78 ± 1.8	26 ± 2	2 (s)	56.3 ± 2.6	21.4 ± 4.6	**87.1 ± 2.0**	**78.6 ± 4.6**		–
EH08-8	4b	266	90 ± 2.2	32 ± 2	2 (s)	62.6 ± 3.4	26.5 ± 6.4	**104.7 ± 3.3**	**73.5 ± 6.4**		–
EH08-9	4a	353	78 ± 1.3	25 ± 1	2 (s)	45.9 ± 4.6	8.7 ± 3.7	**88.8 ± 1.7**	**91.3 ± 3.7**		–
EH08-10	3	383	47 ± 1.0	37 ± 2	3 (m + s)	20.2 ± 1.3	8.1 ± 2.1	39.8 ± 1.3	43.4 ± 4.9	**65.3 ± 2.0**	**48.5 ± 5.0**
EH09-1	3	326	72 ± 2.0	43 ± 2	3 (m + s)	38.8 ± 2.3	19.2 ± 4.2	**71.2 ± 2.8**	**58.6 ± 5.2**	129.4 ± 7.2	22.2 ± 4.6
EH09-2	3	371	60 ± 1.4	38 ± 2	3 (m + s)	34.5 ± 2.3	16.4 ± 5.4	**55.8 ± 2.8**	**55.6 ± 6.1**	94.5 ± 5.1	28.0 ± 5.7
EH09-3	3	307	63 ± 1.7	38 ± 2	3 (m + s)	36.6 ± 3.5	14.9 ± 6.9	**58.0 ± 3.1**	**58.5 ± 7.2**	103.8 ± 6.6	26.6 ± 5.9
EH09-4	3	320	68 ± 1.8	40 ± 2	3 (m + s)	29.0 ± 4.2	5.0 ± 2.7	**56.8 ± 2.0**	**63.7 ± 4.7**	109.5 ± 5.3	31.4 ± 4.8
EH09-10	3	267	77 ± 1.9	31 ± 2	2 (m)	**62.0 ± 2.2**	**56.2 ± 7.2**	102.9 ± 4.9	43.8 ± 7.2		–

Shown are the number of grains used for final D_e determination, the central D_e value calculated for all of the grains and the corresponding overdispersion value. The finite mixture model was used to fit discrete components to each of the D_e distributions. The number of components fitted to the data, the D_e values of these and the proportion of grains belonging to each component are also listed. The D_e values used for age determination are shown in bold.
[a] Indicates whether the D_e distribution was scattered (s) or mixed and scattered (m + s) (see text for details).

(Jacobs et al., 2006a) and the uncertainties in fitting the dose–response curves and the FMM. To this random error, we added (in quadrature) a systematic uncertainty of 2% to allow for possible bias in D_e estimation due to calibration of the $^{90}Sr/^{90}Y$ beta source used for laboratory irradiation of all samples.

Scattered D_e distributions

Nine of the samples collected from El Harhoura 2 and 11 samples from El Mnasra have typical 'scattered' D_e distributions (denoted as (s) in column 6 of Tables 1 and 2), with overdispersion values of between 18 ± 2 and 34 ± 3%. These distributions can be fitted by two discrete D_e components, with the major component containing more than three-quarters of the single-grain D_e values. For the El Harhoura 2 samples, the major component accounts for ≥73% of the D_e values (Table 1), while at El Mnasra it captures ≥89% of the individual estimates (Table 2). The only exception is EM10-1, which contains ~65% of the grains in the major component. The D_e estimates for grains in the minor components are typically about half the value of those in the major components. Most of the samples also have grains with D_e values that fall between these two components.

Such distributions typically result from grains that were buried at the same time, but received different beta doses afterwards. Grains with the lowest D_e values may have received no beta dose, such as when a grain is surrounded by more than 2 mm of low radioactivity material (e.g., carbonate), whereas grains with D_e values intermediate between the two fitted components may have received a partial beta dose, as would occur if they were situated close to a low radioactivity material. The greater abundance of

Table 2
D_e information for all samples measured from El Mnasra.

Sample	Excavation level	No. of grains	Central D_e (Gy)	Overdispersion (%)	No. of components[a]	D_e values (Gy) and proportions (%)					
						Component-1		Component-2		Component-3	
						D_e	Proportion	D_e	Proportion	D_e	Proportion
EM08-1	12 (b)	214	114 ± 2.5	24 ± 2	2 (s)	56.5 ± 4.7	7.4 ± 2.3	**120.9 ± 2.2**	**92.6 ± 2.3**	–	–
EM08-2	12(t)	290	131 ± 2.1	20 ± 2	2 (s)	66.5 ± 7.9	3.3 ± 1.8	**134.5 ± 2.1**	**96.7 ± 1.8**	–	–
EM08-3	11 (t)	365	128 ± 2.1	23 ± 1	2 (s)	57.9 ± 4.8	3.7 ± 1.4	**133.0 ± 1.8**	**96.3 ± 1.4**	–	–
EM08-4	10	336	110 ± 1.8	25 ± 1	2 (s)	58.8 ± 4.7	5.9 ± 2.1	**114.7 ± 1.9**	**94.1 ± 2.1**	–	–
EM08-5	9a	266	119 ± 2.4	26 ± 2	2 (s)	60.1 ± 3.7	6.8 ± 1.9	**125.4 ± 2.0**	**93.3 ± 1.9**	–	–
EM08-6	8	246	116 ± 2.3	25 ± 2	2 (s)	60.0 ± 3.8	5.6 ± 1.8	**122.1 ± 2.0**	**94.4 ± 1.8**	–	–
EM08-7	7b	257	115 ± 1.9	18 ± 2	2 (s)	68.0 ± 5.2	4.8 ± 2.0	**118.7 ± 1.7**	**95.2 ± 2.0**	–	–
EM08-8	6	252	118 ± 2.2	21 ± 2	2 (s)	59.5 ± 6.2	3.6 ± 1.8	**121.8 ± 2.1**	**96.4 ± 1.8**	–	–
EM08-9	6a	388	128 ± 1.8	19 ± 1	2 (s)	83.1 ± 4.4	11.0 ± 3.1	**136.1 ± 2.0**	**89.0 ± 3.1**	–	–
EM08-10	5b	346	106 ± 2.0	29 ± 2	3 (m + s)	18.9 ± 2.2	1.0 ± 0.6	61.0 ± 4.4	7.0 ± 2.2	**113.9 ± 1.8**	**92.0 ± 2.3**
EM08-11	5a	393	53 ± 2.4	89 ± 3	3 (m)	15.4 ± 0.5	28.2 ± 3.0	31.4 ± 2.3	12.5 ± 2.5	**106.9 ± 2.1**	**59.3 ± 2.6**
EM08-12	4 (b)	209	109 ± 3.0	33 ± 2	2 (m)	20.4 ± 2.5	2.5 ± 1.2	**114.4 ± 2.1**	**97.5 ± 1.2**	–	–
EM10-1	3 (t)	229	85 ± 2.3	33 ± 2	2 (s)	61.3 ± 6.2	35.5 ± 14.3	**101.6 ± 6.2**	**64.5 ± 14.3**	–	–
EM10-2	3 (b)	112	81 ± 3.7	40 ± 4	2 (m)	20.4 ± 3.1	4.6 ± 2.3	**88.8 ± 2.8**	**95.4 ± 2.3**	–	–
EM10-3	4	150	84 ± 3.7	47 ± 4	3 (m + s)	21.7 ± 2.6	4.5 ± 2.0	48.4 ± 4.6	16.6 ± 4.6	**104.3 ± 3.4**	**78.9 ± 4.8**
EM10-4	3 (t)	317	49 ± 2.4	82 ± 4	– (m)	Indeterminate					
EM10-5	4 (t)	281	106 ± 2.7	36 ± 2	3 (m + s)	42.5 ± 4.8	5.8 ± 2.2	**97.5 ± 5.7**	**64.3 ± 13.3**	150 ± 14.6	30 ± 13.8
EM10-6	4 (b)	113	120 ± 4.6	34 ± 3	2 (s)	53.4 ± 13.1	4.4 ± 3.5	**126.5 ± 3.9**	**95.6 ± 3.5**	–	–

Shown are the number of grains used for final D_e determination, the central D_e value calculated for all of the grains and the corresponding overdispersion value. The finite mixture model was used to fit discrete components to each of the D_e distributions. The number of components fitted to the data, the D_e values of these and the proportion of grains belonging to each component are also listed. The D_e values used for age determination are shown in bold.
[a] Indicates whether the D_e distribution was scattered (s), mixed (m) or mixed and scattered (m + s) (see text for details).

inhomogeneous carbonate indurations at El Harhoura 2 may explain the greater proportion of grains (up to 27%) in the minor D_e component of those samples. We argue against mixing as the mechanism responsible for generating these types of D_e distributions, because the proportion of grains in the two D_e components remains similar down a single stratigraphic profile (~3.5 m deep at El Harhoura 2 and ~2.7 m deep at El Mnasra), which is not consistent with mixing as a result of particle diffusion (Heimsath et al., 2002). Also, the taphonomic study of microvertebrates by Stoetzel et al. (2011b) demonstrated that there has been little disturbance of these deposits. For samples with 'scattered' D_e distributions, therefore, the layers from which they were collected are thought to have retained their stratigraphic integrity and not been compromised by post-depositional mixing.

We used the approach described by Jacobs et al. (2008b, c) to identify those samples that have a spread in D_e values consistent with beta dose variations between grains, and classified 20 of the 30 samples as having 'scattered' distributions. For each of these samples, the OSL age was calculated from the weighted mean D_e of the major component (i.e., the component containing the greatest proportion of grains, as determined by the FMM: Tables 1 and 2) divided by the D_r with the beta dose rate adjusted for the proportion of grains in the main component (Tables 3 and 4). Worked examples of this approach are given in Jacobs et al. (2011), together with a sensitivity test to demonstrate the limited effect that our assumptions, and the use of modelled beta dose rates, have on the final ages. Fig. 5 shows a representative example of a scattered D_e distribution for each site.

Mixed D_e distributions

Six samples from El Harhoura 2 and seven samples from El Mnasra have been identified as having possible 'mixed' or 'mixed and scattered' D_e distributions. These samples are identified as (m) or (m + s) in column six of Tables 1 and 2. Two or three D_e components could be fitted to these distributions using the FMM. The D_e overdispersion values range from 31 ± 2 to 43 ± 2% at El Harhoura 2 (Table 1) and from 29 ± 2 to 89 ± 3% at El Mnasra (Table 2), which are significantly greater than the corresponding ranges for the 'scattered' D_e distributions (with the sole exception of EH08-8). These D_e distributions typically contain a proportion of measured grains that can be interpreted as intrusive, given that the spread in D_e values is too large to be explained solely in terms of grain-to-grain variations in beta dose rate. We envisage that sediment mixing took place by a combination of natural processes and anthropogenic factors. Representative examples of 'mixed and scattered' D_e distributions for samples from El Harhoura 2 and El Mnasra are shown in Fig. 6a and b, respectively.

At El Mnasra, the samples with 'mixed' and 'mixed and scattered' distributions are from the latest MP and purported UP (Levels 3, 4, 5a and 5b). For samples EM08-10, EM08-12, EM10-2 and EM10-3, the FMM identified a low-D_e component (centred on ~20 Gy) that consists of only a few grains (1–5% of the total number). We consider these grains as intrusive. Their corresponding ages are 16–20 ka, using the dose rates for the levels in which these grains finally came to rest (Table 4). When these few grains are removed from the data sets, the four D_e distributions assume the appearance and overdispersion properties of the El Mnasra samples with 'scattered' D_e distributions.

Sample EM08-11, however, contained a much higher proportion of intrusive grains (~40%). The most likely explanation for this scatter may be the presence of an ancient animal burrow that could have been penetrated during sample collection, resulting in grains with different burial ages being mixed together. The existence of many large burrows throughout the deposit provides a compelling case to use single-grain analyses and finite mixture modelling to identify intrusive grains. These issues cannot be resolved using conventional multi-grain aliquots (Arnold and Roberts, 2009). But even single-grain analyses and the FMM failed to untangle the D_e distribution of sample EM10-4, which is mixed to such an extent that discrete components could not be reliably fitted (Fig. 7). It is likely that the deposit at the point of sampling was heavily disturbed, possibly by a burrowing animal. For such D_e distributions, it is feasible to calculate maximum and minimum burial ages for the sediments, but the relationship of these ages to the cultural or human remains is open to question.

At El Harhoura 2, the six samples with possible 'mixed' or 'mixed and scattered' D_e distributions are restricted to the latest MP (Level 3). The four Level 3 samples collected along the southern, western and northern excavation walls (EH09-1, -2, -3 and -4; Fig. 2c) have the same type of D_e distribution (Fig. S1). In each case, three D_e components were identified, with the middle D_e component represented by the largest proportion of grains (56–64%) and the highest D_e component by 22–31% of the grains. The latter grains have similar D_e values to those in the underlying MP layers (Table 3), which suggest that they may be derived from the underlying deposits, but the mixing mechanism is not clear. Alternatively, or in addition, roof spall contamination might explain the upper range of D_e values, but is unlikely to account for the full range of D_e values encompassed by this component. But in either case, the intrusive grains making up this component should be removed prior to final D_e and age calculation.

Table 3
Equivalent dose (D_e) and dose rate values used to calculate the OSL ages of the El Harhoura 2 samples.

Sample	Excavation level	Moisture content (%)	Adjusted beta dose rate (Gy/ka)	Gamma dose rate (Gy/ka)	Cosmic-ray dose rate (Gy/ka)	Total dose rate (Gy/ka)	Final D_e value (Gy)	Age (ka)
EH08-1	11	8 ± 2	0.54 ± 0.04	0.31 ± 0.01	0.04 ± 0.01	0.92 ± 0.05	114.0 ± 2.3	123.7 ± 7.4
EH08-2	10	8 ± 2	0.57 ± 0.04	0.35 ± 0.01	0.04 ± 0.01	0.99 ± 0.05	117.0 ± 2.7	118.3 ± 7.1
EH08-3	9	5 ± 1	0.58 ± 0.04	0.37 ± 0.01	0.05 ± 0.01	1.04 ± 0.05	111.9 ± 2.0	108.1 ± 5.9
EH08-4	8	5 ± 1	0.57 ± 0.04	0.34 ± 0.01	0.05 ± 0.01	0.99 ± 0.05	105.8 ± 3.5	106.7 ± 6.6
EH08-5	7	5 ± 1	0.48 ± 0.03	0.30 ± 0.01	0.05 ± 0.01	0.87 ± 0.04	93.7 ± 2.6	108.1 ± 6.3
EH08-6	6	5 ± 1	0.41 ± 0.03	0.29 ± 0.01	0.05 ± 0.01	0.79 ± 0.04	91.8 ± 2.2	116.4 ± 6.6
EH08-7	5	5 ± 1	0.44 ± 0.03	0.32 ± 0.01	0.06 ± 0.01	0.85 ± 0.04	87.1 ± 2.0	102.6 ± 5.7
EH08-8	4b	5 ± 1	0.58 ± 0.03	0.38 ± 0.01	0.06 ± 0.01	1.05 ± 0.05	104.7 ± 3.3	99.9 ± 5.8
EH08-9	4a	5 ± 1	0.64 ± 0.04	0.37 ± 0.01	0.07 ± 0.01	1.11 ± 0.05	81.8 ± 1.7	73.7 ± 4.1
EH08-10	3	3 ± 1	0.63 ± 0.03	0.31 ± 0.01	0.09 ± 0.01	1.06 ± 0.05	65.3 ± 2.0	61.9 ± 3.5
EH09-1	3	9 ± 2	0.64 ± 0.04	0.36 ± 0.01	0.12 ± 0.01	1.15 ± 0.04	71.2 ± 2.8	61.9 ± 4.1
EH09-2	3	6 ± 2	0.56 ± 0.03	0.37 ± 0.01	0.12 ± 0.01	1.08 ± 0.05	55.8 ± 2.8	51.6 ± 3.6
EH09-3	3	6 ± 2	0.51 ± 0.03	0.35 ± 0.01	0.12 ± 0.01	1.01 ± 0.05	58.0 ± 3.1	57.7 ± 4.2
EH09-4	3	7 ± 2	0.58 ± 0.04	0.35 ± 0.01	0.12 ± 0.01	1.06 ± 0.05	56.8 ± 2.0	52.6 ± 3.3
EH09-10	3	15 ± 4	0.62 ± 0.04	0.34 ± 0.01	0.09 ± 0.01	1.08 ± 0.07	62.0 ± 2.2	57.3 ± 4.2

Table 4
Equivalent dose (D_e) and dose rate values used to calculate the OSL ages of the El Mnasra samples.

Sample	Excavation level	Moisture content (%)	Adjusted beta dose rate (Gy/ka)	Gamma dose rate (Gy/ka)	Cosmic-ray dose rate (Gy/ka)	Total dose rate (Gy/ka)	Final D_e value (Gy)	Age (ka)
EM08-1	12 (base)	3 ± 1	0.39 ± 0.03	0.29 ± 0.01	0.14 ± 0.01	0.86 ± 0.04	113.9 ± 2.3	133.2 ± 7.0
EM08-2	12 (upper)	9 ± 2	0.60 ± 0.04	0.34 ± 0.01	0.15 ± 0.01	1.11 ± 0.06	134.5 ± 2.2	121.0 ± 6.9
EM08-3	11 (upper)	12 ± 3	0.71 ± 0.05	0.34 ± 0.01	0.15 ± 0.01	1.23 ± 0.07	133.0 ± 1.8	108.3 ± 6.6
EM08-4	10	9 ± 2	0.59 ± 0.04	0.29 ± 0.01	0.15 ± 0.01	1.06 ± 0.06	114.7 ± 1.9	108.5 ± 6.3
EM08-5	9a	7 ± 2	0.68 ± 0.04	0.29 ± 0.01	0.15 ± 0.02	1.12 ± 0.06	125.4 ± 2.0	108.9 ± 6.2
EM08-6	8	7 ± 2	0.57 ± 0.04	0.29 ± 0.01	0.15 ± 0.02	1.05 ± 0.05	122.1 ± 2.0	116.7 ± 6.4
EM08-7	7b	14 ± 4	0.46 ± 0.03	0.45 ± 0.01	0.15 ± 0.02	1.09 ± 0.06	118.7 ± 1.7	108.8 ± 6.6
EM08-8	6	15 ± 4	0.57 ± 0.04	0.34 ± 0.01	0.16 ± 0.02	1.09 ± 0.07	121.8 ± 2.1	111.6 ± 7.3
EM08-9	6a	6 ± 2	0.72 ± 0.04	0.36 ± 0.01	0.16 ± 0.02	1.27 ± 0.06	136.1 ± 2.0	107.4 ± 5.8
EM08-10	5b	13 ± 3	0.54 ± 0.04	0.33 ± 0.01	0.16 ± 0.02	1.06 ± 0.06	113.9 ± 1.8	107.5 ± 6.6
EM08-11	5a	11 ± 3	0.50 ± 0.03	0.32 ± 0.01	0.16 ± 0.02	1.00 ± 0.05	106.9 ± 2.1	106.5 ± 6.5
EM08-12	4 (base)	20 ± 5	0.57 ± 0.04	0.34 ± 0.01	0.16 ± 0.02	1.11 ± 0.07	114.4 ± 2.1	103.5 ± 7.5
EM10-1	3 (upper)	14 ± 4	0.71 ± 0.04	0.44 ± 0.04	0.17 ± 0.02	1.35 ± 0.09	101.6 ± 2.3	75.3 ± 5.6
EM10-2	3 (base)	13 ± 3	0.67 ± 0.04	0.49 ± 0.03	0.17 ± 0.02	1.36 ± 0.09	97.4 ± 2.9	71.6 ± 5.3
EM10-3	4	35 ± 9	0.54 ± 0.04	0.37 ± 0.03	0.16 ± 0.02	1.10 ± 0.11	104.0 ± 3.4	94.6 ± 9.7
EM10-4	3 (upper)	11 ± 3	0.64 ± 0.04	0.44 ± 0.03	0.17 ± 0.02	1.28 ± 0.09	Indeterminate	
EM10-5	4 (upper)	20 ± 5	0.48 ± 0.04	0.34 ± 0.02	0.16 ± 0.02	1.02 ± 0.08	97.5 ± 5.7	95.4 ± 9.3
EM10-6	4 (base)	25 ± 6	0.52 ± 0.04	0.37 ± 0.03	0.16 ± 0.02	1.08 ± 0.09	115.3 ± 3.0	106.7 ± 9.6

The third, and lowest, D_e component is represented by 5–20% of the grains (Table 1). These D_e values are not dissimilar to those obtained for samples collected from Level 2 (the UP Iberomaurusian; data not reported here). A layer of large roof fall (Fig. 2c) forms a distinct boundary that clearly delimits Level 3 from Level 2 along the southern, northern and western faces of the excavation. When we collected these four samples, three of them (EH09-1, EH09-2 and EH09-4) were deliberately taken from beneath some of the large blocks of fallen roof rock (Fig. 2c), which we assumed would have provided protection against the downward movement of younger, overlying sediments. The fourth sample (EH09-3) was also collected from the northern face, but at a position where there is a clear stratigraphic separation between Levels 3 and 2.

So, what was the mechanism responsible for producing the component with the smallest D_e values? Wasp activity has been observed, in the form of small burrowing holes along the excavation walls. These appear to be more prevalent in section walls excavated previously than in freshly excavated sections, which suggests that such activity is a recent, post-excavation occurrence. If this is the case, then wasp activity should not be a significant problem. It may introduce some zero-age (modern) grains from the surface of the wall, but such grains would be recognized and removed using our single-grain procedures, and any mixing would occur horizontally within Level 3, resulting in the admixture of grains with similar burial ages. We did, however, clean the section walls prior to sampling and could not identify any zero-age grains in any of our samples, which suggests that the smallest D_e values are due to some other factor(s).

A more likely explanation for the low-D_e grains is the effect of variations in the beta dose rate to individual grains. The sediments at the front of the cave are partially indurated with carbonate, and carbonate conglomerates have formed around most of the bones and stones. Carbonates are low in radioactivity compared to most other minerals, so the low-D_e component may represent carbonate-coated grains that received a smaller beta dose during burial than did grains in the middle and high-D_e components. To calculate appropriate ages for these samples, the grains in the high-D_e component were removed from the data sets and the remaining D_e values were then treated in the same way as for the 'scattered' distributions. Two discrete D_e components were fitted to these data and the main D_e component was used for age estimation. Our treatment of the D_e data sets for Level 3 is consistent, therefore, with that of samples collected from the deeper levels, where post-depositional disturbance is not an issue. In practical terms, this approach does not produce significantly different ages to those

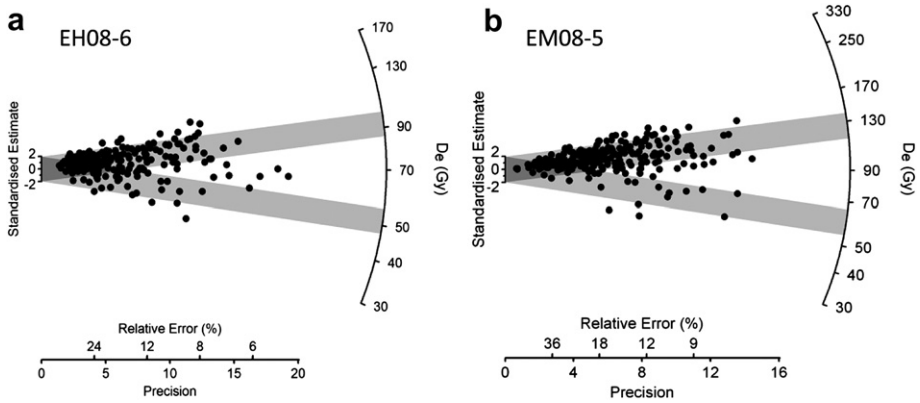

Figure 5. Representative radial plots of 'scattered' single-grain D_e distributions from a) El Harhoura 2 and b) El Mnasra. The grey bands are centred on the central D_e values for the major and minor components, which were fitted using the 'finite mixture model'. Each point represents the D_e value for a single grain and can be read by extending a line from zero on the standardised estimate axis through the point of interest, to intersect the radial axis. The relative error on this D_e is read by projecting a line to intersect the horizontal axis. The precision is the reciprocal of the relative error, so that the most precise D_e estimates fall on the right-hand side of such plots.

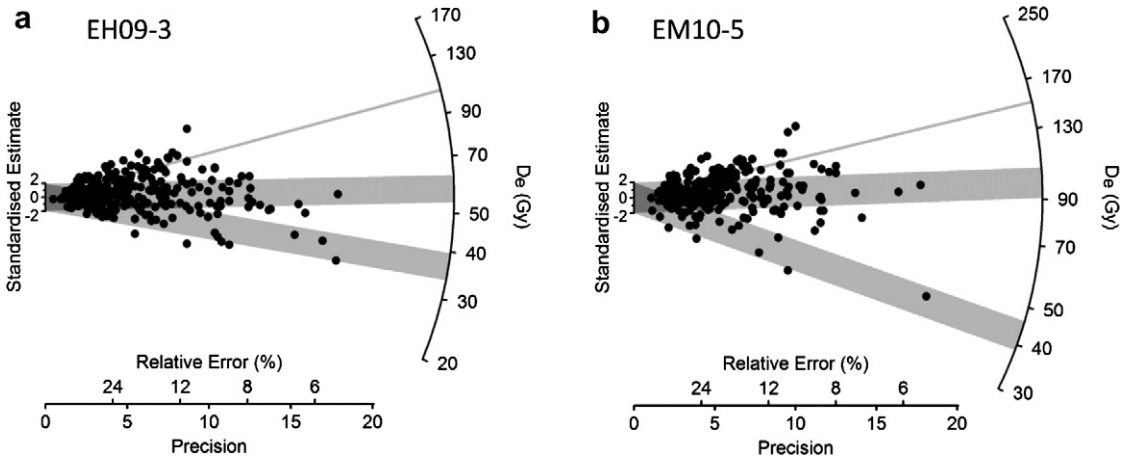

Figure 6. Representative radial plots of 'mixed and scattered' single-grain D_e distributions from a) El Harhoura 2 and b) El Mnasra. The grey bands are centred on the central D_e values for the major component and for the component interpreted to be the result of small-scale differences in the beta dose rate to individual grains. The solid grey lines are centred on the central D_e of a third component, identified using the finite mixture model, and interpreted as representing mixed-in and intrusive grains.

obtained under the assumption that the smaller D_e values represent intrusive grains (see, for example, the sensitivity test in supporting online information in Jacobs et al., 2011), but it does have implications for the stratigraphic integrity of the cultural and skeletal remains recovered from Level 3.

Two other samples from Level 3 were collected from less secure stratigraphic positions. Sample EH08-10 was collected from along the eastern section wall (Fig. 2d), where there is clear evidence for massive Neolithic pits that could have caused significant disturbance of the underlying layers. The D_e distribution for this sample also consists of three D_e components. Two of these occur in approximately equal proportions and have similar weighted mean D_e values (65.3 $\pm$ 2.0 and 39.8 $\pm$ 1.3 Gy) to the two lowest D_e components obtained for the other Level 3 samples. The third component has a much smaller D_e value ($\sim$20 Gy) and is thought to represent intrusive grains from the overlying Level 2; using the measured D_r for this sample (Table 3) gives an age of $\sim$19 ka for this component, which is similar to the ages obtained for the low-D_e intrusive grains at El Mnasra. Interestingly, there is no discernable input from the Neolithic in sample EH08-10, despite the extensive pit-digging observed in this area. For consistency with the other samples from Level 3, the main D_e component was used to estimate its age, and the D_r was corrected for beta-dose heterogeneity.

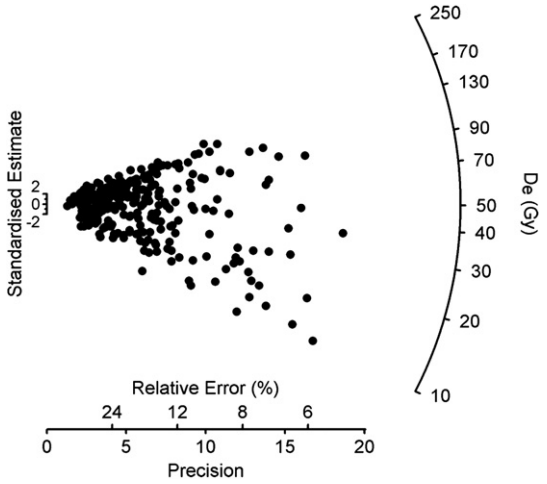

Figure 7. The 'mixed' D_e distribution obtained for sample EM10-4 (Level 3) from El Mnasra. This radial plot shows a D_e distribution for which an accurate age could not be obtained. For such samples, the stratigraphic integrity of the associated cultural and human remains is open to question.

The sixth sample from Level 3 (EH09-10) was collected from the base of the sedimentary sequence in the cavity at the rear of the cave (Fig. 2a). The Level 3 deposits here are $\sim$10 cm thick and perched on a rock, but it is not known whether the rock represents bedrock or is just a large fallen slab. Only two D_e components (62 $\pm$ 2 and 103 $\pm$ 5 Gy) were identified (Table 1). The component with the smallest D_e values contains a slightly higher proportion of grains, and its weighted mean D_e value is consistent with those obtained from the dominant (middle) D_e component of samples from Level 3 at the front of the cave; we used this component for age determination of sample EH09-10. By contrast, the higher D_e component consists of values similar to those obtained for samples from the earlier part of the MP. These grains, therefore, may be derived from older, and as yet unexcavated, sediments beneath the rock, or may represent unbleached or partially bleached grains produced by disintegration of the slab of rock and released into the overlying Level 3 sediments.

It is interesting that sample EH09-10 lacks a third component with much smaller D_e values, because thick UP and Neolithic deposits overlie the thin Level 3 sediments at this location. The absence of such a component implies no significant mixing, despite evidence for considerable disturbance of the overlying Level 2 deposits. The absence of small D_e values also suggests that the effect of variations in the beta dose received by individual grains is not problematic in this instance, which is compatible with field observations of few carbonates and no induration of the sediments. The close agreement between the ages of sample EH09-10 and the other Level 3 samples from the front of the cave can be viewed as providing independent validation of the beta-dose correction procedure employed for the latter samples.

Environmental dose rate measurements

The dose rate for each sample represents the sum of the beta and gamma dose rates due to ^{238}U, ^{235}U, ^{232}Th (and their decay products) and ^{40}K. The bulk beta and gamma dose rates were measured by GM-25-5 low-level beta counting (Bøtter-Jensen and Mejdahl, 1988) and in situ gamma-ray spectrometry, respectively. Allowance was made for beta dose attenuation (Mejdahl, 1979), HF acid etching (Bell and Zimmerman, 1978) and sample water content

(Aitken, 1985). The moisture contents used for age determination were based on the field values at the time of sample collection, which range from 3 to 15% at El Harhoura 2 (Table 3) and from 3 to 35% at El Mnasra (Table 4). The El Mnasra values are more variable because of differences in the sedimentological properties of the samples: Those with the lowest water contents are sandy and free-draining, whereas those with the higher water contents contain significant amounts of silts, clays and ash. We consider the measured water contents as representative of the long-term water contents for these samples, as the cave is quite humid and the deposit damp throughout.

In contrast, the El Harhoura 2 deposit was fairly dry throughout (water contents of 3–9%), except in the small cavity at the back of the cave (~15%). The sediments at the front of the cave were also much more compacted than those in the rear cavity and at El Mnasra. The deposit at the front of the cave is only slightly protected from weather and is fully exposed to direct sunlight, so it has probably always retained only a small amount of moisture. The deposit in the rear cavity is comparatively humid, completely protected from sunlight, and some speleothems have formed as a result of water percolating through the cave roof. Its higher measured water content is, therefore, also thought to be representative of the long-term average. For all of the El Harhoura 2 and El Mnasra samples, we allowed for a relative uncertainty of ±25% (at 1σ) on the water contents to accommodate the likely range of values experienced by the sediments since deposition; the OSL ages increase by ~1% for each 1% increase in water content.

The cosmic-ray dose rates were calculated following Prescott and Hutton (1994), and included adjustments for site altitude (19 m for El Harhoura 2 and 14 m for El Mnasra), geomagnetic latitude (38.7°), density and thickness of cave rock (2.5 g/cm^3) and sediment (1.8 g/cm^3) overburden, and the $\cos^2\Phi$ zenith angle dependence of cosmic rays (Smith et al., 1997). We also assumed an effective internal alpha dose rate of 0.03 ± 0.01 Gy/ka, which falls within the range of measured values for acid-etched quartz grains from different locations (Feathers and Migliorini, 2001; Bowler et al., 2003; Jacobs et al., 2003b).

By estimating the beta and gamma dose rates from beta counting and field gamma spectrometry, we have assumed that the present state of (dis)equilibrium in the U and Th decay chains has prevailed throughout the burial period of each sample. These emission-counting methods are, however, superior to those that determine only the parental U concentration (e.g., neutron activation analysis or ICP-MS), as the latter are critically dependent on the assumption of secular equilibrium in the ^{238}U chain. By contrast, even the most common time-dependent disequilibria in the ^{238}U chain are unlikely to lead to relative errors in D_r of more than a few percent when emission-counting techniques are employed (Olley et al., 1996, 1997).

We note that the total dose rate exhibits only modest variation at both sites, showing no trend with depth in the stratigraphy or location within each cave. The gamma dose rates range between 0.29 and 0.38 Gy/ka at El Harhoura 2, and from 0.29 to 0.45 Gy/ka at El Mnasra. These estimates take into account any inhomogeneities in the gamma-ray sphere at each sample location. Greater variability is observed in the beta dose rates: 0.41–0.62 Gy/ka at El Harhoura 2 and 0.39–0.72 Gy/ka at El Mnasra. There is no practicable way to obtain an estimate of the beta dose rate for each of the measured individual grains. In the laboratory, an average beta dose rate for the bulk sample is obtained and this is assumed to be representative for every grain measured. We have argued that this assumption is not valid for the sediments from El Harhoura 2 and El Mnasra, based on the distribution of D_e values for each of the samples. In such cases, the grains used to calculate the sample D_e require their beta dose rates to be adjusted appropriately, which we achieved using the procedure described by Jacobs et al. (2008c). This approach is based on the appearance of the D_e distribution and the identification of two D_e components by the FMM (Tables 1 and 2). The component comprised of the lower D_e values may represent grains that received little or no beta dose in their burial environment, as a consequence of them being juxtaposed or encased by low radioactivity materials (e.g., carbonate). The FMM allows an estimate to be made of the proportion of grains influenced by such materials, and the beta dose rate for the other D_e component (from which the age is determined) can be adjusted accordingly. Additional details, and worked examples, are given in Jacobs et al. (2008c, 2011) and Haslam et al. (2011). This beta-dose correction was made to all samples, except for EH09-10 (which was collected from the cavity at the rear of El Harhoura 2) and EM10-4 (for which an age could not be calculated).

The dose rate information for each sample is presented in Tables 3 and 4. The uncertainty associated with the total dose rate of each sample represents the quadratic sum of all known and estimated sources of random and systematic error.

Age estimates

To obtain an age for each sample, its D_e value was divided by the corresponding D_r value listed in Table 3 (El Harhoura 2) and 4 (El Mnasra). These tables also list the single-grain OSL ages and their 1σ uncertainties, derived by combining in quadrature the uncertainties on the D_e and D_r estimates.

El Harhoura 2 We were able to obtain reliable ages for all of the samples collected from the MP levels at El Harhoura 2. The two basal samples collected from the archaeologically sterile Levels 11 and 10 (EH08-1 and -2) gave ages of 124 ± 7 ka and 118 ± 7 ka. These are consistent with each other and indicate sediment deposition during MIS 5e. The ages of the six samples collected from Levels 9 to 4b (EH08-3 to -8) range between 116 ± 7 and 100 ± 6 ka. These are statistically indistinguishable at 2σ. The samples from Levels 8, 6 and 4b are associated with the Aterian, whereas those from Levels 7 and 5 are archaeologically sterile.

There appears to be a discernible break in time between Levels 4b and 4a. The sample collected from the latter level (EH08-9) gives an age of 74 ± 4 ka, which is significantly different from the age of the underlying Level 4b. The archaeological and faunal contents of these two sub-levels are usually combined and attributed to the Aterian, but the OSL ages suggest that these sub-levels are not contemporaneous and, therefore, their contents should not be combined for analysis. There is then another hiatus between Levels 4a and 3 (the latest MP). Six samples were collected from Level 3, five from the front and one from the rear of the cave, which gave ages of between 62 ± 4 ka (EH08-10, EH09-1) and 52 ± 4 ka (EH09-2). Part of this spread probably reflects the uncertainty in untangling the mixing observed for some of these samples (Figs. 6a and S1) and in correcting the beta dose rate for the proportion of grains affected by carbonate cementation after burial.

To further resolve the chronology for the site, we used the statistical (homogeneity) test of Galbraith (2003) to determine if the independent ages obtained for Level 3, and those for Levels 9 to 4b, are self-consistent (i.e., the spread in ages are statistically compatible with the size of the age uncertainties). The test assumes that the OSL ages are independent observations sampled from a log-normal distribution, and the null hypothesis is that the ages are consistent with a common value. We recognize that this test should be used to compare multiple estimates of age for a specific event (i.e., the same level such as for Level 3), whereas we are also comparing age estimates for sediments possibly deposited over several centuries, millennia or longer (i.e., ages from Levels 9 to 4b). Such time intervals will be hard to discern if they are shorter than

the size of the individual age uncertainties. In the present context, therefore, we are using the homogeneity test to establish if the spread in ages is sufficiently narrow that the null hypothesis cannot be rejected when the age uncertainties are taken into account. The latter outcome would indicate that the ages of the relevant layer or layers are consistent with either a single event or with sediment accumulation over a time span commensurate with the size of the age uncertainties (i.e., several millennia at 1σ).

The calculated *P*-values (which indicate the probability that a random value from a chi-squared distribution with $n-1$ degrees of freedom is greater than the homogeneity test statistic, G) are $P = 0.094$ and $P = 0.44$ for Level 3 and Levels 9 to 4b, respectively. A small *P*-value (by convention <0.05) indicates that the ages are not all compatible with a common value. The *P*-values for the two groups, however, are greater than 0.05, which supports the null hypothesis and suggests that the OSL ages are self-consistent within each group. Accordingly, we calculated a weighted mean age of 56.9 ± 2.2 ka for the samples from Level 3 and a weighted mean age of 106.5 ± 3.1 ka for the ages from Levels 9 to 4b, under the assumption that the individual age estimates represent either a single event or a series of events spread over a time interval that is short compared to the size of the age uncertainties.

El Mnasra We also obtained reliable age estimates for all, but one, of the samples from El Mnasra. Two ages were obtained for Level 12, a yellow brown sand at the base of the excavation, which represents a marine sand thought to be associated with the last interglacial (MIS 5e) sea level at 126 ± 2 ka (e.g., Waelbroeck et al., 2008). An age of 133 ± 7 ka (EM08-1) was obtained for the base of Level 12, and an age of 121 ± 7 ka (EM08-2) from ~72 cm higher in the section, near the top of Level 12 (Fig. 3b). These ages are consistent with sediment deposition during a sea-level transgression at the end of MIS 6 and during MIS 5e, and with the ages obtained for the lowermost deposits at El Harhoura 2.

EM08-3 was collected from Level 11 (the lowest expression of the Aterian), and gave an age of 108 ± 7 ka. From this level up to the base of Level 4 in the deep trench (EM08-12), all ages are statistically indistinguishable at 2σ, including the ages for samples collected from archaeological sterile levels interspersed with levels containing the Aterian. The OSL ages range between 117 ± 6 ka (EM08-6) and 104 ± 8 ka (EM08-12). A weighted mean age of 108.9 ± 2.9 ka ($P = 0.95$) was calculated for these ten samples. This provides a reliable and precise estimate of the time of first occurrence, and the strongest expression, of the Aterian at El Mnasra. These individual age estimates for the Aterian, and the weighted mean, are consistent with those for Aterian occupation of El Harhoura 2, but they are not sufficiently precise to resolve periods of site occupation and abandonment that lasted for only a few millennia, or less.

The three other samples collected from Level 4 have similar or slightly younger ages. In the deep trench, Level 4 consists of one thick ash band, but along the eastern wall and above the current excavation to the west of the deep trench in areas B and C in Fig. 3a, this level appears to split into at least two layers, seen as additional white ash bands. The sample collected from the lowermost exposed ash band along the eastern wall was dated to 107 ± 10 ka (EM10-6), consistent with the age for the base of Level 4 in the deep trench (104 ± 8 ka). The sample collected from the uppermost exposed ash band gave an age of 95 ± 9 ka (EM10-5), which is consistent with the age of 95 ± 10 ka obtained for the intermediate sample, EM10-3. It is probable, therefore, that there is some time transgression between the base and top of Level 4 and, hence, for the Aterian at this site, but the ages are all statistically consistent. A similar relationship between sample age and stratigraphic position was also observed for the Aterian deposits at Contrebandiers (Jacobs et al., 2011). When all the ages for the Aterian represented in Levels 11 and 7–4 are combined, a weighted mean age of 106.2 ± 3.0 ka ($P = 0.92$) is obtained, which is almost identical to the weighted mean ages for the Aterian at El Harhoura 2 (this study) and Contrebandiers (Jacobs et al., 2011).

We also obtained ages for Level 3, which has been tentatively attributed to the UP. Towards the front of the cave, the contact between these sediments and the underlying Level 4 deposits is relatively diffuse and the Level 3 deposits are heavily disturbed by pits, with the base represented by a bioturbated layer ~20 cm thick. Accordingly, we did not collect an OSL sample from this layer. The upper part of Level 3 is better preserved in the back of the cave, where a sharp contact is visible between these and the overlying Level 2 (Neolithic) deposits. At this location, Level 3 consists of two dark, organic-rich layers separated and overlain by reddish sediments. The ages for the lower and upper black lenses (72 ± 5 and 75 ± 6 ka, respectively) are indistinguishable, but no age could be determined for the sample collected from the overlying red sediment (EM10-4). The D_e distribution for this sample (Fig. 7) shows that these sediments have been heavily bioturbated and include grains that were last exposed to sunlight between 95 and 7 ka ago. Based on the weighted mean age of 73.3 ± 4.2 ka for the two other samples from Level 3 (EM10-1 and -2), it would appear that the sediments (and, hence, the associated artefacts) were not deposited during the UP, but are time-equivalent to the Aterian assemblage from Level 4a at El Harhoura 2. As Level 3 at El Mnasra has not been excavated by the current excavation team, and there is no documentation that the previous excavators found UP artefacts, we consider it likely that the UP is not present at El Mnasra. Instead, we suggest that the MP is overlain directly by the Neolithic, but the nature of the final MP remains to be demonstrated. This issue may be resolved by ongoing excavations, geoarchaeological investigations and additional OSL dating of these deposits.

Schwenninger et al. (2010) also calculated OSL ages for four sediment samples from El Mnasra (X2413–X2316). These ages can be compared directly with those obtained in this study, because the samples were collected from the same profile in the deep trench; their locations are shown as stars in Fig. 3b. Samples X2413 and X2414 were collected from Level 12 and produced ages of 119 ± 20 and 112 ± 7 ka, respectively, which are similar to our single-grain ages of 133 ± 7 ka (EM08-1) and 121 ± 7 ka (EM08-2). Sample X2415 was collected from Level 7b and was dated to 108 ± 8 ka (consistent with 109 ± 7 ka for EM08-7), while sample X2416 was collected from Level 5a and gave an age of 106 ± 12 ka (consistent with the single-grain age of 107 ± 7 ka for EM08-11). Both sets of ages indicate the relatively short time span represented by the sediments accumulated in Levels 12 to 4 in the deep trench at El Mnasra.

In summary, the single-grain ages obtained in this study for samples collected from El Mnasra and El Harhoura 2 reveal periods of occupation of both sites between about 110 and 95 ka, and at ~75 ka. A late MP occupation of El Harhoura 2 is also recorded at ~55 ka. These OSL chronologies confirm other recent reports of Aterian assemblages in Morocco dating to more than 100 ka (Barton et al., 2009; Richter et al., 2010; Schwenninger et al., 2010; Jacobs et al., 2011).

Discussion

Archaeological chronologies

OSL ages are now available from five sites in the Témara region, on the Atlantic coast of Morocco. The age estimates obtained from four dating studies (Barton et al., 2009; Schwenninger et al., 2010; Jacobs et al., 2011; and this study) are summarized in Fig. 8, with

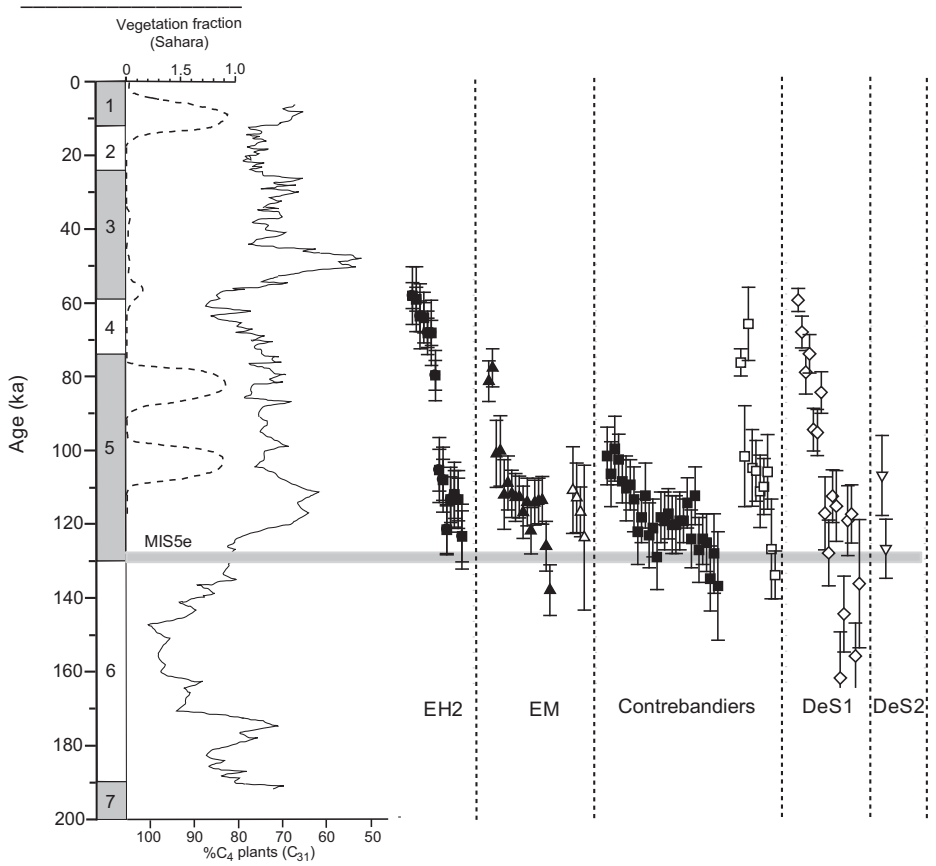

Figure 8. OSL ages for sediments deposited at archaeological sites in the Rabat-Témara area, Atlantic coast of Morocco, together with palaeoenvironmental reconstructions based on sediment cores collected from off the northwest coast of Africa. The left-hand dashed line indicates the relative cover of grassland vegetation in the western Sahara over the last 120 ka deduced from grain-size analysis of marine sediments (Tjallingii et al., 2008). The adjacent continuous trace denotes the relative abundance of C_4 plants (warm-season grasses and sedges) inferred from the isotopic composition of long-chain (C_{31}) n-alkanes in leaf waxes derived from the central Sahara/Sahel region (Castañeda et al., 2009). The OSL ages for each site (abbreviations: EH2, El Harhoura 2; EM, El Mnasra; DeS1, Dar es-Soltan 1; DeS2, Dar es-Soltan 2) are plotted in stratigraphic order. Ages indicated with solid symbols were obtained using single-grain OSL dating (this study and Jacobs et al., 2011), whereas ages displayed with open symbols were obtained from multi-grain aliquots (Barton et al., 2009; Schwenninger et al., 2010). Marine Isotope Stages (and sub-stages MIS 5e, 5c and 5a) are indicated next to the age axis.

the ages arranged in stratigraphic order for each site. This site synthesis reveals a number of important chronological features:

1) The basal levels from all five sites are approximately the same age (130–120 ka) and are consistent with deposition during the MIS 5e high sea level at ~126 ka (Waelbroeck et al., 2008). Some older ages have been determined for sediments from Dar es-Soltan 1, but these are either inconsistent with their stratigraphic positions (i.e., younger sediments are found beneath these samples, as is the case with X2379, X2396 and X2376), or the associated uncertainties are sufficiently large that these ages are statistically consistent with those of the basal samples from the other sites. Such ages may result from contamination of samples by grains derived from decomposed roof spall, and the inability to identify and discard such grains from multi-grain aliquots before sample D_e and age determination.
2) The oldest evidence of human occupation is found in Level L at Dar es-Soltan 1. A multi-grain OSL age of 112 ± 8 ka was measured, but this was increased to 130 ± 6 ka by fitting a Bayesian model to the stratigraphic sequence of OSL ages (Barton et al., 2009; Schwenninger et al., 2010). At Contrebandiers, the lowermost archaeological deposits (Layer 6c) have a weighted mean age of 122 ± 5 ka (Jacobs et al., 2011).
3) All five sites were then occupied from ~110 to 95 ka, but it is not clear from the current chronologies whether occupation was relatively continuous over this interval, or was punctuated by two or more discrete pulses of occupation, separated by periods of site abandonment. The former seems more likely, based on the single-grain OSL chronologies obtained for El Harhoura 2 and El Mnasra in this study and for Contrebandiers by Jacobs et al. (2011). At present, the temporal resolution achievable by OSL dating is insufficient to allow estimates of duration of a few millennia or less, but more finely-resolved sampling may shed further light on this.
4) Some of the sites (but not Contrebandiers or Dar es-Soltan 2) contain sediments dated to between 80 and 70 ka with archaeological traces. The artefact attributions, however, are inconsistent between the sites. Those at El Mnasra have been assigned to the UP, whereas the contemporaneous assemblages at El Harhoura 2 and Dar es-Soltan 1 have been classified as MP. Resolution of this issue requires further investigations into the stratigraphic integrity of the deposits and the association between the dated sediments and the archaeological materials found within them. Interestingly, assemblages of this antiquity are contemporaneous with Aterian deposits excavated at cave sites in northeastern Morocco (e.g., Taforalt: Bouzouggar et al., 2007; Ifri n'Ammar: Richter et al., 2010; Rhafas: Mercier et al., 2007).
5) Thus far, sediments with archaeological traces identified as MP, and dated to between ~60 and 50 ka in the Témara region,

have been found only at El Harhoura 2 and Dar es-Soltan 1. At the latter site, this age interval encompasses both the uppermost Aterian found in Ruhlmann's Unit C[2] and what he termed the 'Devolved Mousterian' in Unit C[1] (Ruhlmann, 1951; Barton et al., 2009). Closer scrutiny of these artefact assemblages (together with single-grain dating of the deposits to validate the multi-grain ages) may help inform whether the Aterian was the final MP industry in Morocco, or if other, as yet poorly understood, industries existed prior to the start of the UP. MP deposits dated to 55–45 ka, and to 30–20 ka, have also been identified and dated at Taforalt (Bouzouggar et al., 2007).

Human–environment interactions

The three age clusters identified for human occupation of the Témara caves may hold clues to the influence of past environments on human habitation, migration and site abandonment in the region. Why was human occupation of these sites sporadic? There are no continuous terrestrial records in the Témara area from which climatic information for the Late Pleistocene can be gleaned, but sediment cores collected from off the northwest coast of Africa provide relevant data for this time period (Tjallingii et al., 2008; Castañeda et al., 2009). Tjallingii et al. (2008) developed a humidity index and vegetation cover model for the Sahara and Sahel regions of northwestern Africa (Fig. 8), based on grain-size analyses of siliciclastic minerals deposited off the coast of Mauritania by aeolian and fluvial processes, combined with a fully coupled atmosphere–ocean–vegetation model. Greater fluvial input implies greater humidity, whereas a greater relative input of wind-blown dust indicates a drier environment. The modelled regions do not geographically overlap with the Rabat-Témara area, but the changes observed in these records would likely have had an impact due to the position of Rabat-Témara along the eastern boundary of the North Atlantic current, a major forcing mechanism of Northern Hemisphere (and global) climate change. For example, Tjallingii et al. (2008) found a strong correlation between millennial-scale dry events and the occurrence of Greenland stadial and Heinrich events that have been related to North Atlantic freshwater pulses and a greatly reduced North Atlantic meridional overturning circulation. Castañeda et al. (2009) used a different marine core, collected ~1100 km further south, to measure the carbon-isotope composition of individual plant leaf waxes derived from the central Sahara/Sahel region. From this isotopic information, they reconstructed changes in the relative abundance of C_3 and C_4 plants (primarily shrubs/trees and grasses, respectively) over the last 192 ka (Fig. 8).

In the Tjallingii et al. (2008) reconstruction, the three wettest periods of the last 120 ka peaked at ~105 ka (MIS 5c), ~83 ka (MIS 5a) and ~10 ka, which are coincident with the largest orbital precession peaks in African monsoonal forcing. The onset of these wet periods is too rapid, however, to be explained solely by gradual insolation forcing, but can be simulated by incorporating changes in vegetation cover. Tjallingii et al. (2008) proposed that the three periods of enhanced humidity were associated with significant expansions in grassland habitat across the Sahara, and with grass and tree cover in the Sahel. Based on these model simulations, the MIS 5c and MIS 5a wet periods may have been characterized by a rainfall regime and vegetation cover similar to those that prevailed during the well-known African Humid Period (the interval from 15 to 6 ka), when the Sahara was covered in lush grass and littered with lakes (deMenocal et al., 2000; Gasse, 2000).

Castañeda et al. (2009) also observed periods of enhanced humidity, at 120–110 ka (MIS 5d), 55–45 ka and ~10 ka, in an isotopic record that shows central North Africa was dominated by arid conditions (and C_4 plants) for most of the last 190 ka. The wetter conditions encouraged the expansion of C_3 vegetation, which was even more abundant (relative to C_4 grasses) during the MIS 5d and MIS 3 humid episodes than during the African Humid Period. Castañeda et al. (2009) did not observe humid pulses during MIS 5c or MIS 5a, but Tjallingii et al. (2008) identified a modest increase in vegetation cover between 60 and 55 ka, with the remainder of MIS 3 characterized by abrupt millennial-scale alternations between arid and humid events. The latter fluctuations are also recorded in two sediment cores collected from the western Mediterranean Sea, north of Morocco (Nebout et al., 2002; Moreno et al., 2005). These millennial-scale climatic events have been linked to oscillations in winter rainfall associated with changes in the strength of the North Atlantic meridional overturning circulation, which is thought to control the distribution of vegetation in northwest and central North Africa (Tjallingii et al., 2008; Castañeda et al., 2009).

There are some clear correlations between the wet episodes identified by Tjallingii et al. (2008) and Castañeda et al. (2009) and the MP occupations of the three Témara caves dated with the single-grain OSL technique. El Harhoura 2, El Mnasra and Contrebandiers were occupied by Aterian toolmakers between about 110 and 95 ka, which falls near the end of the MIS 5d humid period in the Castañeda et al. (2009) record and coincides with the MIS 5c humid pulse in the Tjallingii et al. (2008) reconstruction. Of these three sites, only Contrebandiers preserves evidence of earlier human occupation, during MIS 5e. The Tjallingii et al. (2008) reconstruction does not encompass the last interglacial, but it may be significant that the longer record of Castañeda et al. (2009) indicates that MIS 5e was not especially wet.

El Harhoura 2 and El Mnasra were subsequently occupied at ~73 ka, near the end of the MIS 5a wet period identified by Tjallingii et al. (2008). The single-grain OSL ages for El Harhoura 2, El Mnasra and Contrebandiers suggest site abandonment (or the lack of deposition or preservation of sediments) during MIS 4, a period that Castañeda et al. (2009) considered the most severe of the entire Late Pleistocene. The weighted mean age of 57 ± 2 ka for the latest MP occupation of El Harhoura 2 falls near the start of MIS 3 and is compatible with site reoccupation during the wet period that peaked 60–55 ka ago (Tjallingii et al., 2008: Fig. 9) or 55–45 ka ago (Castañeda et al., 2009). The 55–45 ka humid episode is the most prominent of the entire Late Pleistocene in the Castañeda et al. (2009) isotopic record, but is much less pronounced in the reconstruction by Tjallingii et al. (2008), perhaps because the latter site does not capture the climate signal from the North African interior (Castañeda et al., 2009). Further studies are required to confirm its strength and geographic extent.

This suggestion of occupation of sites along the Atlantic coast of Morocco in response to wet phases, when climates were most favourable and grassland habitats expanded dramatically, supports an earlier proposal by Marean and Assefa (2005) that populations of Aterian people moved with grasslands, following the expanded habitat as it spread into coastal and inland areas. The microfaunal assemblage from El Harhoura 2 also supports this model. Stoetzel et al. (2011b) reported that palaeoecological data deduced from the micromammal assemblages in the archaeological levels (3, 4a, 6 and 8) implied a relatively humid climate and a landscape vegetated mainly by open grassland, with some wooded or bushy areas and available freshwater. The archaeologically sterile Levels 5 and 7, however, told a different story. The Level 5 micromammal assemblage indicated a cooler and more arid climate, while the Level 7 assemblage showed evidence of further climatic deterioration, resulting in a steppe landscape lacking available freshwater. These interpretations are supported by analyses of the macrofaunal remains from El Harhoura 2 and other sites in the region. The faunal assemblages in Levels 5 and 7 accumulated in the 110–100 ka time

interval and may reflect millennial-scale dry events during MIS 5c, similar to those identified for MIS 3, but too short-lived to be resolved by OSL dating. This same caveat applies to human occupation of these sites, where archaeological visibility is low and people likely used them only as short-term, seasonal camps.

Conclusions

The archaeological sequences at El Harhoura 2 and El Mnasra provide further insights into the timing and duration of the MP, particularly the Aterian, in western Morocco. By measuring and analysing the OSL signals from individual grains of quartz, it has proven possible to obtain reproducible and accurate OSL ages. The single-grain OSL chronologies of both sites suggest that they were occupied episodically, punctuated by periods of site abandonment. Based on a comparison with two continuous records of Late Pleistocene climate and vegetation (as reconstructed from the grain-size and carbon-isotope compositions of sediment cores off the northwest coast of Africa), it appears that the 3 episodes of human occupation can be correlated with contemporaneous phases of wetter climate and expanded grassland habitat; the gaps in occupation may represent drier periods and a contraction of grassland in the Sahara. The main stimulus for occupation, therefore, may be related to changes in rainfall and vegetation associated with events in the North Atlantic Ocean, which has been proposed as a major control on millennial-scale aridity and humidity in northwest and central North Africa. We still lack high-resolution archaeological records and terrestrial archives of past environments for this region, but the temporal patterns emerging from these new chronologies may help to answer some of the unresolved questions and facilitate comparisons between broadly contemporaneous faunal and artefact assemblages from different sites. Future research could usefully focus on testing our interpretations using a wider range of environmental proxies from these and other sites in the region.

Acknowledgements

The majority of this research was funded by the Australian Research Council through Discovery Project grants DP0666084 to Roberts and Jacobs and DP1092843 to Jacobs. We would like to specially thank the Institut National des Sciences de l'Archéologie et du Patrimoine and its Director, Dr Aomar Akerraz, the Ministry of Culture of Morocco, and the Mission archéologique El Harhoura-Témara, funded by the Commission consultative des recherches archéologiques à l'étranger of Ministère des Affaires Etrangères (France). Part of the fieldwork was also funded by the French Agence Nationale de la Recherche, 'La 6eme Extinction, MOHMIE' Program, ANR-09-PEXT-004 (dir. C. Denys). We also thank all members of the excavation and research teams for valuable information that has helped us to understand and interpret the OSL data.

Appendix. Supplementary material

Supplementary material associated with this article can be found, in the online version, at doi:10.1016/j.jhevol.2011.12.001.

References

Aitken, M.J., 1985. Thermoluminescence Dating. Academic Press, London.
Aitken, M.J., 1998. An Introduction to Optical Dating. Oxford University Press, Oxford.
Arnold, L.J., Roberts, R.G., 2009. Stochastic modelling of multi-grain equivalent dose (D_e) distributions: implications for OSL dating of sediment mixtures. Quatern. Geochronol. 4, 204–230.
Aumassip, G., 2001. Le concept Moustérien en Afrique du nord. L'Homme Maghrébin et son Environnement Depuis 100 000 Ans. Actes du Colloque International de Maghnia. Centre National de Recherches Préhistoriques, Anthropologiques et Historiques, Alger, pp. 89–100.
Bailey, R.M., 2003. Paper I: the use of measurement-time dependent single-aliquot equivalent-dose estimates from quartz in the identification of incomplete signal resetting. Radiat. Meas. 37, 673–683.
Bailey, R.M., 2004. Paper I—simulation of dose absorption in quartz over geological timescales and its implications for the precision and accuracy of optical dating. Radiat. Meas. 38, 299–310.
Bailey, R.M., Armitage, S.J., Stokes, S., 2005. An investigation of pulsed-irradiation regeneration of quartz OSL and its implications for the precision and accuracy of optical dating (Paper II). Radiat. Meas. 39, 347–359.
Ballarini, M., Wintle, A.G., Wallinga, J., 2006. Spatial variation of dose rates from beta sources as measured using single grains. Ancient TL 24, 1–8.
Balter, M., 2011. Was North Africa the launch pad for modern human migration? Science 331, 20–23.
Barton, R.N.E., Bouzouggar, A., Collcutt, S.N., Schwenninger, J.-L., Clark-Balzan, L., 2009. OSL dating of the Aterian levels at Dar es-Soltan I (Rabat, Morocco) and implications for the dispersal of modern *Homo sapiens*. Quatern. Sci. Rev. 28, 1914–1931.
Bell, W.T., Zimmerman, D.W., 1978. The effect of HF acid etching on the morphology of quartz inclusions for thermoluminescence dating. Archaeometry 20, 63–65.
Bordes, F., 1976. Moustérien et Atérien. Quaternaria 19, 19–34.
Bøtter-Jensen, L., Bulur, E., Duller, G.A.T., Murray, A.S., 2000. Advances in luminescence instrument systems. Radiat. Meas. 32, 523–528.
Bøtter-Jensen, L., McKeever, S.W.S., Wintle, A.G., 2003. Optically Stimulated Luminescence Dosimetry. Elsevier, Amsterdam.
Bøtter-Jensen, L., Mejdahl, V., 1988. Assessment of beta dose-rate using a GM multicounter system. Nucl. Tracks Rad. Meas. 14, 187–191.
Bouzouggar, A., Barton, N., Vanhaeren, M., d'Errico, F., Collcutt, S., Higham, T., Hodge, E., Parfitt, S., Rhodes, E., Schwenninger, J.L., Stringer, C., Turner, E., Ward, S., Moutmir, A., Stambouli, A., 2007. 82,000-year-old shell beads from North Africa and implications for the origins of modern human behaviour. Proc. Natl. Acad. Sci. 104, 9964–9969.
Bowler, J.M., Johnston, H., Olley, J.M., Prescott, J.R., Roberts, R.G., Shawcross, W., Spooner, N.A., 2003. New ages for human occupation and climatic change at Lake Mungo, Australia. Nature 421, 837–840.
Campmas, E., 2007. Etude taphonomique et archéozoologique du materiel faunique de la grotte d'El Harhoura 2 (Témara, Maroc). Master Dissertation, Université Bordeaux.
Campmas, E., Michel, P., Amani, F., Cochard, D., Costamango, S., Nespoulet, R., El Hajraoui, M.A., 2008. Comportements de subsistance à l'Atérien et au Néolithique au Maroc Atlantique: premiers résultats de l'étude taphonomique et archéozoologique des faunes d'El Harhoura 2 (Région de Témara, Maroc). In: Actes de la Quatrième Rencontre des Quaternaristes Marocains, Oujda, pp. 236–254.
Camps, G., 1974. Les Civilisations Préhistoriques de l'Afrique du Nord et du Sahara. Doin, Paris.
Castañeda, I.S., Mulitza, S., Schefuß, E., Lopes dos Santos, R.A., Sinninghe Damsté, J.S., Schouten, S., 2009. Wet phases in the Sahara/Sahel region and human migration patterns in North Africa. Proc. Natl. Acad. Sci. 106, 20159–20163.
David, B., Roberts, R.G., Magee, J., Mialanes, J., Turney, C., Bird, M., White, C., Fifield, L.K., Tibby, J., 2007. Sediment mixing at Nonda Rock: investigations of stratigraphic integrity at an early archaeological site in northern Australia and implications for the human colonisation of the continent. J. Quatern. Sci. 22, 449–479.
Debénath, A., 1975. Découverte de restes humains probablement Atériens à Dar es Soltane (Maroc). C.R. Acad. Sci. D 281, 875–876.
Debénath, A., 1976. Le site de Dar-es-Soltane 2, à Rabat (Maroc). Bull. Mém. Soc. Anthropol. Paris 3, 181–182.
Debénath, A., 1980. Nouveaux restes humains Atériens du Maroc. C.R. Acad. Sci. Paris 290, 851–852.
Debénath, A., 1992. Hommes et cultures matérielles de l'Atérien Marocain. L'Anthropologie 96, 711–720.
Debénath, A., 2000. Le peuplement préhistorique du Maroc: données récentes et problèmes. L'Anthropologie 104, 131–145.
Debénath, A., Sbihi-Alaoui, F.Z., 1979. Découverte de deux nouveaux gisements préhistoriques près de Rabat (Maroc). Bull. Soc. Préhist. Fr 76, 11–14.
deMenocal, P., Ortiz, J., Guilderson, T., Adkins, J., Sarntheim, N., Baker, L., Yarusinsky, M., 2000. Abrupt onset and termination of the African humid period: rapid climate response to gradual insolation forcing. Quatern. Sci. Rev. 19, 347–361.
d'Errico, F., Vanhaeren, M., Barton, N., Bouzouggar, A., Mienis, H., Richter, D., Hublin, J.-J., McPherron, S.P., Lozouet, P., 2009. Additional evidence on the use of personal ornaments in the Middle Paleolithic of North Africa. Proc. Natl. Acad. Sci. 106, 16051–16056.
Drake, N.A., Blench, R.M., Armitage, S.J., Bristow, C.S., White, K.H., 2011. Ancient watercourses and biogeography of the Sahara explain the peopling of the desert. Proc. Natl. Acad. Sci. 108, 458–462.
Duller, G.A.T., 2003. Distinguishing quartz and feldspar in single grain luminescence measurements. Radiat. Meas. 37, 161–165.
El Hajraoui, M.A., 1993. Nouvelles découvertes Néolithiques et Atériennes dans la region de Rabat (Grotte d'El Mnasra). Mediterraneô 2, 105–121.
El Hajraoui, M.A., 1994. L'industrie osseuse Atérienne de la grotte d'El Mnasra (Région de Témara, Maroc). Préhist. Anthropol. Méditerranéennes 3, 91–94.

El Hajraoui, M.A., 2004. Le Paléolithique du domaine mésetien septentrional. Données récentes sur le littoral: Rabat, Témara et la Mamora. Ph.D. Dissertation, Université Mohamed.
Feathers, J.K., 2003a. Use of luminescence dating in archaeology. Meas. Sci. Technol. 14, 1493–1509.
Feathers, J.K., 2003b. Single-grain OSL dating of sediments from the Southern High Plains, USA. Quatern. Sci. Rev. 22, 1035–1042.
Feathers, J.K., Migliorini, E., 2001. Luminescence dating at Katanda—a reassessment. Quatern. Sci. Rev. 20, 961–966.
Galbraith, R.F., 2003. A simple homogeneity test for estimates of dose obtained using OSL. Ancient TL 21, 75–77.
Galbraith, R.F., Roberts, R.G., Laslett, G.M., Yoshida, H., Olley, J.M., 1999. Optical dating of single grain and multiple grains of quartz from Jinmium rock shelter, northern Australia: Part I, experimental design and statistical models. Archaeometry 41, 339–364.
Gasse, F., 2000. Hydrological changes in the African tropics since the last glacial maximum. Quatern. Sci. Rev. 19, 189–211.
Haslam, M., Roberts, R.G., Shipton, C., Pal, J.N., Fenwick, J.L., Ditchfield, P., Boivin, N., Dubey, A.K., Gupta, M.C., Petraglia, M., 2011. Late Acheulean hominins at the Marine Isotope Stage 6/5e transition in north-central India. Quatern. Res. 75, 670–682.
Heimsath, A.M., Chappell, J., Spooner, N.A., Questiaux, D.G., 2002. Creeping soil. Geology 30, 111–114.
Henshilwood, C.S., d'Errico, F., Vanhaeren, M., Van Niekerk, K., Jacobs, Z., 2004. Middle Stone Age shell beads from South Africa. Science 304, 404.
Howe, B., 1967. The Palaeolithic of Tangier, Morocco: excavations at Cape Ashakar, 1939–1947. Bull. Am. Sch. Prehist. Res. 22, 1–200.
Hublin, J.-J., 1992. Recent human evolution in northwestern Africa. In: Aitken, M., Mellars, P., Stringer, C.B. (Eds.), The Origin of Modern Humans, the Impact of Science-Based Dating. Phil. Trans. R. Soc. 337, 185–191.
Hublin, J.-J., 2001. Northwestern African Middle Pleistocene hominids and their bearing on the emergence of Homo sapiens. In: Barham, L., Robson-Brown, K. (Eds.), Human Roots. Africa and Asia in the Middle Pleistocene. CHERUB, Western Academic and Specialist Press Ltd, Bristol, pp. 99–121.
Hublin, J.-J., Tillier, A.-M., Tixier, J., 1987. L'humérus d'enfant Moustérien (Homo 4) du Djebel Irhoud (Maroc) dans son contexte archéologique. Bull. Mém. Soc. Anthropol. Paris 4, 115–141.
Jacobs, Z., 2010. An OSL chronology for the sedimentary deposits from Pinnacle Point Cave 13B – a punctuated presence. J. Hum. Evol. 59, 289–305.
Jacobs, Z., Duller, G.A.T., Wintle, A.G., 2003a. Optical dating of dune sand from Blombos Cave, South Africa: II - single grain data. J. Hum. Evol. 44, 613–625.
Jacobs, Z., Duller, G.A.T., Wintle, A.G., 2006a. Interpretation of single grain D_e distributions and calculation of D_e. Radiat. Meas. 41, 264–277.
Jacobs, Z., Duller, G.A.T., Wintle, A.G., Henshilwood, C.S., 2006b. Extending the chronology of deposits at Blombos Cave, South Africa, back to 140 ka using optical dating of single and multiple grains of quartz. J. Hum. Evol. 51, 255–273.
Jacobs, Z., Meyer, M.C., Roberts, R.G., Aldeias, V., Dibble, H., El Hajraoui, M.A., 2011. Single-grain OSL dating at La Grotte des Contrebandiers ('Smugglers' Cave'), Morocco: improved age constraints for the Middle Paleolithic levels. J. Archaeol. Sci. 38, 3631–3643.
Jacobs, Z., Roberts, R.G., 2007. Advances in optically stimulated luminescence dating of individual grains of quartz from archeological deposits. Evol. Anthropol. 16, 210–223.
Jacobs, Z., Roberts, R.G., 2008. Testing times: old and new chronologies for the Howieson's Poort and Still Bay industries in environmental context. S. Afr. Archaeol. Soc. Goodwin Ser. 10, 9–34.
Jacobs, Z., Roberts, R.G., Galbraith, R.F., Deacon, H.J., Grün, R., Mackay, A., Mitchell, P., Vogelsang, R., Wadley, L., 2008a. Ages for the Middle Stone Age of southern Africa: implications for human behavior and dispersal. Science 322, 733–735.
Jacobs, Z., Wintle, A.G., Duller, G.A.T., 2003b. Optical dating of dune sand from Blombos Cave, South Africa: I – multiple grain data. J. Hum. Evol. 44, 599–612.
Jacobs, Z., Wintle, A.G., Duller, G.A.T., Roberts, R.G., Wadley, L., 2008b. New ages for the post-Howiesons Poort, late and final Middle Stone Age at Sibudu, South Africa. J. Archaeol. Sci. 35, 1790–1807.
Jacobs, Z., Wintle, A.G., Roberts, R.G., Duller, G.A.T., 2008c. Equivalent dose distributions from single grains of quartz at Sibudu, South Africa: context, causes and consequences for optical dating of archaeological deposits. J. Archaeol. Sci. 35, 1808–1820.
Jain, M., Murray, A.S., Bøtter-Jensen, L., 2003. Characterisation of blue-light stimulated luminescence components in different quartz samples: implications for dose measurement. Radiat. Meas. 37, 441–449.
Lombard, M., Wadley, L., Jacobs, Z., Mohapi, M., Roberts, R.G., 2010. Still Bay and serrated points from Umhlatuzana Rock Shelter, Kwazulu-Natal, South Africa. J. Archaeol. Sci. 37, 1773–1784.
Marean, C.W., Assefa, Z., 2005. The Middle and Upper Pleistocene African record for the biological and behavioral origins of modern humans. In: Stahl, A. (Ed.), African Archaeology: A Critical Introduction. Blackwell Publishing Ltd, Malden, pp. 93–129.
McBrearty, S., Brooks, A.S., 2000. The revolution that wasn't: a new interpretation of the origin of modern human behavior. J. Hum. Evol. 39, 453–563.
McBurney, C.B.M., 1975. Current status of the Lower and Middle Palaeolithic of the entire region from the Levant through North Africa. In: Wendorf, F., Marks, A.E. (Eds.), Problems in Prehistory: North Africa and the Levant. Southern Methodist University Press, Dallas, pp. 411–423.
Mejdahl, V., 1979. Thermoluminescence dating: beta-dose attenuation in quartz grains. Archaeometry 21, 61–72.
Mercier, N., Wengler, L., Valladas, H., Joron, J.L., Froget, L., Reyss, J.-L., 2007. The Rhafas Cave (Morocco): chronology of the Mousterian and Aterian archaeological occupations and their implications for Quaternary geochronology based on luminescence (TL/OSL) age determinations. Quatern. Geochronol. 2, 309–313.
Michel, P., Campmas, E., Stoetzel, E., Nespoulet, R., El Hajraoui, M.A., 2009. La macrofaune du Pléistocène Supérieur d'El Harhoura 2 (Témara, Maroc): données preliminaries. L'Anthropologie 113, 283–312.
Michel, P., Campmas, E., Stoetzel, E., Nespoulet, R., El Hajraoui, M.A., Amani, F., 2010. La grande faune du Paléolithique Supérieur (niveau 2) et du Paléolithique Moyen (niveau 3) de la grotte d'El Harhoura 2 (Témara, Maroc): étude paléontologique, reconstitutions paléoécologiques et paléoclimatiques. Hist. Biol. 22, 327–340.
Monchot, H., Aouraghe, H., 2009. Deciphering the taphonomic history of an Upper Paleolithic faunal assemblage from Zouhrah Cave/El Harhoura 1, Morocco. Quaternaira 20, 239–253.
Moreno, A., Cacho, I., Canals, M., Grimalt, J.O., Sánchez-Goñi, M.F., Shackleton, N., Sierro, F.J., 2005. Links between marine and atmospheric processes oscillating on a millennial time-scale. A multi-proxy study of the last 50,000 yr from the Alboran Sea (Western Mediterranean Sea). Quatern. Sci. Rev. 24, 1623–1636.
Murray, A.S., Roberts, R.G., 1997. Determining the burial time of single grains of quartz using optically stimulated luminescence. Earth Planet. Sci. Lett. 152, 163–180.
Nebout, N.C., Turon, J.L., Zahn, R., Capotondi, L., Londeix, L., Pahnke, K., 2002. Enhanced aridity and atmospheric high-pressure stability over the western Mediterranean during the North Atlantic cold events of the past 50 k.y. Geology 30, 863–866.
Nespoulet, R., El Hajraoui, M.A., Amani, F., Ben Ncer, A., Debénath, A., El Idrissi, A., Lacombe, J.-P., Michel, P., Oujaa, A., Stoetzel, E., 2008. Palaeolithic and Neolithic occupations in the Témara region (Rabat, Morocco): recent data on hominin contexts and behavior. Afr. Archaeol. Rev. 25, 21–39.
Niftah, S., 2003. Contribution à l'étude stratigraphique, sédimentologique et micromorphologique des remplissages du Pléistocène Supérieur des grottes du littoral Atlantique Marocain (El Mnasra, les Contrebandiers et El Harhoura II, région de Témara, Rabat). Ph.D. Dissertation, Université de Perpignan.
Niftah, S., Debénath, A., Miskovsky, J.-C., 2005. Origine du remplissage sédimentaire des grottes de Témara (Maroc) d'aprés l'étude des minéraux lourds et l'étude exoscopique des grains de quartz. Quaternaira 16, 73–83.
Olley, J.M., Murray, A.S., Roberts, R.G., 1996. The effects of disequilibria in the uranium and thorium decay chains on burial dose rates in fluvial sediments. Quatern. Sci. Rev. 15, 751–760.
Olley, J.M., Roberts, R.G., Murray, A.S., 1997. Disequilibria in the uranium decay series in sedimentary deposits at Allen's Cave, Nullarbor Plain, Australia: implications for dose rate determinations. Radiat. Meas. 27, 433–443.
Osborne, A.H., Vance, D., Rohling, E.J., Barton, N., Rogerson, M., Fello, N., 2008. A humid corridor across the Sahara for the migration of early modern humans out of Africa 120,000 years ago. Proc. Natl. Acad. Sci. 105, 16444–16447.
Prescott, J.R., Hutton, J.T., 1994. Cosmic ray contributions to dose rates for luminescence and ESR dating: large depths and long term time variations. Radiat. Meas. 23, 497–500.
Reygasses, M., 1919–1920. Etudes de palethnologie Maghrébine (nouvelle série). Recueil des Notices et Mémoires de la Société Archéologique. Historique et Géographique de Constantine 52, 513–570.
Richter, D., Moser, J., Nami, M., Eiwanger, J., Mikdad, A., 2010. New chronometric data from Ifri n'Ammar (Morocco) and the chronostratigraphy of the Middle Palaeolithic in the Western Maghreb. J. Hum. Evol. 59, 672–679.
Roberts, R.G., Bird, M., Olley, J., Galbraith, R., Lawson, E., Laslett, G., Yoshida, H., Jones, R., Fullagar, R., Jacobsen, G., Hua, Q., 1998. Optical and radiocarbon dating at Jinmium rock shelter in northern Australia. Nature 393, 358–362.
Roberts, R.G., Galbraith, R.F., Olley, J.M., Yoshida, H., Laslett, G.M., 1999. Optical dating of single and multiple grains of quartz from Jinmium rock shelter, northern Australia: part II, results and implications. Archaeometry 41, 365–395.
Roberts, R.G., Galbraith, R.F., Yoshida, H., Laslett, G.M., Olley, J.M., 2000. Distinguishing dose populations in sediment mixtures: a test of single-grain optical dating procedures using mixtures of laboratory-dosed quartz. Radiat. Meas. 32, 459–465.
Roche, J., 1969. Fouilles de la grotte des Contrebandiers (Maroc). Palaeoecol. Afr. 4, 120–121.
Roche, J., 1976. Chronostratigraphie des restes Atériens de la grotte des Contrebandiers à Témara (Province de Rabat). Bull. Mém. Soc. Anthropol. Paris, 165–173.
Roche, J., Texier, J.-P., 1976. Découverte de restes humains dans un niveau Atérien supérieur de la grotte des Contrebandiers, à Temara (Maroc). C.R. Acad. Sci. 282, 45–47.
Ruhlmann, A., 1951. La Grotte Préhistorique de Dar es-Soltan. Larose, Paris.
Schwenninger, J.-L., Colcutt, S.N., Barton, R.N.E., Bouzouggar, A., El Hajraoui, M.A., Nespoulet, R., Debénath, A., 2010. A new luminescence chronology for Aterian cave sites on the Atlantic coast of Morocco. In: Garcea, E.E.A. (Ed.), Southeastern Mediterranean Peoples between 130,000 and 10,000 Years Ago. Oxbow Books, Oxford.
Singarayer, J.S., Bailey, R.M., 2003. Further investigations of the quartz optically stimulated luminescence components using linear modulation. Radiat. Meas. 37, 451–458.
Smith, M.A., Prescott, J.R., Head, M.J., 1997. Comparison of ^{14}C and luminescence chronologies at Puritjarra rock shelter, central Australia. Quatern. Sci. Rev. 16, 299–320.

Stoetzel, E., 2009. Les microvertébrés du site d'occupation humaine d'El Harhoura 2 (Pléistocène Supérieur – Holocène, Maroc): systématique, évolution, taphonomie et paléoécologie. Ph.D. Dissertation, Muséum National d'histoire Naturelle, Sciences de la Nature et de l'Homme, Paris.

Stoetzel, E., Denys, C., Bailon, S., El Hajraoui, M.A., Nespoulet, R., 2011a. Taphonomic analysis of amphibian and squamate remains from El Harhoura 2 (Rabat-Témara, Morocco): contributions to palaeocological and archaeological interpretations. Int. J. Osteoarchaeol.. doi:10.1002/oa.1275.

Stoetzel, E., Marion, L., Nespoulet, R., El Hajraoui, M.A., Denys, C., 2011b. Taphonomy and palaeoecology of the late Pleistocene to middle Holocene small mammal succession of El Harhoura 2 cave (Rabat-Témara, Morocco). J. Hum. Evol. 60, 1–33.

Texier, J.P., Raynal, J.P., Lefevre, D., 1985. Nouvelles propositions pour un cadre chronologique du Quaternaire Marocain. C.R. Acad. Sci. 301, 183–188.

Tixier, J., 1959. Les pièces pédonculées de l'Atérien, VI–VII. Lybica, pp. 127–158.

Tjallingii, R., Claussen, M., Stuut, J.W., Fohlmeister, J., Jahn, A., Bickert, T., Lamy, F., Röhl, U., 2008. Coherent high- and low-latitude control of the northwest African hydrological balance. Nat. Geosci. 1, 670–675.

Tribolo, C., Mercier, N., Rasse, M., Soriano, S., Huysecom, E., 2010. Kobo 1 and L'Abri aux Vaches (Mali, West Africa): two case studies for the optical dating of bioturbated sediments. Quatern. Geochronol. 5, 317–323.

Vanhaeren, M., d'Errico, F., Stringer, C., James, S.L., Todd, J.A., Mienis, H.K., 2006. Middle Paleolithic shell beads in Israel and Algeria. Science 312, 1785–1788.

Waelbroeck, C., Frank, N., Jouzel, J., Parrenin, F., Masson-Delmotte, V., Genty, D., 2008. Transferring radiometric dating of the last interglacial sea level high stand to marine and ice core records. Earth Planet. Sci. Lett. 265, 183–194.

Wendorf, F., Schild, R., Close, A., 1993. Egypt during the Last Interglacial: The Middle Paleolithic of Bir Tarfawi and Bir Sahara East. Plenum Press, New York.

Wintle, A.G., 2008. Fifty years of luminescence dating. Archaeometry 50, 276–312.

Wrinn, P.J., Rink, W.J., 2003. ESR dating of tooth enamel from Aterian levels at Mugharet el 'Aliya (Tangier, Morocco). J. Archaeol. Sci. 30, 123–133.

Yoshida, H., Roberts, R.G., Olley, J.M., Laslett, G.M., Galbraith, R.F., 2000. Extending the age range of optical dating using single 'supergrains' of quartz. Radiat. Meas. 32, 439–446.